ADVANCED MATERIALS
www.advmat.de

Slip-Stacked J-Aggregate Materials for Organic Solar Cells and Photodetectors

*Jin Hong Kim, Tim Schembri, David Bialas, Matthias Stolte, and Frank Würthner**

This paper is dedicated to Prof. Daoben Zhu on the occasion of his 80th birthday

Dye–dye interactions affect the optical and electronic properties in organic semiconductor films of light harvesting and detecting optoelectronic applications. This review elaborates how to tailor these properties of organic semiconductors for organic solar cells (OSCs) and organic photodiodes (OPDs). While these devices rely on similar materials, the demands for their optical properties are rather different, the former requiring a broad absorption spectrum spanning from the UV over visible up to the near-infrared region and the latter an ultra-narrow absorption spectrum at a specific, targeted wavelength. In order to design organic semiconductors satisfying these demands, fundamental insights on the relationship of optical properties are provided depending on molecular packing arrangement and the resultant electronic coupling thereof. Based on recent advancements in the theoretical understanding of intermolecular interactions between slip-stacked dyes, distinguishing classical J-aggregates with predominant long-range Coulomb coupling from charge transfer (CT)-mediated or -coupled J-aggregates, whose red-shifts are primarily governed by short-range orbital interactions, is suggested. Within this framework, the relationship between aggregate structure and functional properties of representative classes of dye aggregates is analyzed for the most advanced OSCs and wavelength-selective OPDs, providing important insights into the rational design of thin-film optoelectronic materials.

1. Introduction

The impact of aggregation on functional properties has been discussed controversially in the past. Thus, dye aggregation has been considered as detrimental for a variety of functions such as fluorescence[1] or photocurrent generation in dye-sensitized solar cells.[2] Meanwhile, however, an increasing community is aware of the benefits of aggregation to tune the functional properties of π-conjugated materials toward specific needs.[3–6] In this regard, photophysical studies for small model dimers demonstrate how redox properties, singlet and triplet energies as well as orientation and distance determine the fate of the optically excited state and how tailored spacer and substituent units can be used to tune the respective photoexcited aggregate state toward fluorescence, phosphorescence, charge separation, or singlet fission.[7,8] Translation of this knowledge into supramolecularly engineered solid-state materials appears as the logical next step.[9] Here, it needs to be considered that ordered arrangements over long distances are only ensured in the crystalline state, while disorder and grain size will have a considerable impact on the properties of common thin film materials.[10,11] It is accordingly not yet a common strategy to tailor organic solid-state materials by considering the expected packing arrangements and their impact on the functional properties, i.e., supramolecular engineering, and instead in most research only molecular properties are designed and the successful packing arrangements depend on serendipity. Furthermore, insights into the respective molecular arrangements in noncrystalline thin-film materials are not trivial to acquire by experimental methods and often rely on the interpretation of changes in the UV-vis–NIR (near-infrared) absorption spectra by simple theories like the molecular exciton model and the interpretation in terms of H- and J-aggregates.[12] Comprehensive research has been conducted to improve the understanding of various aspects of optoelectronic devices such as organic solar cells (OSCs) and organic photodiodes (OPDs) including charge generation and electronic processes within such devices[13,14] as well as recent efforts on elucidating intermolecular charge transfer states in bulk heterojunction (BHJ) devices.[15,16] Nevertheless,

J. H. Kim, T. Schembri, M. Stolte, F. Würthner
Center for Nanosystems Chemistry (CNC) and Bavarian Polymer Institute (BPI)
Universität Würzburg
Theodor-Boveri-Weg, 97074 Würzburg, Germany
E-mail: wuerthner@uni-wuerzburg.de
D. Bialas, M. Stolte, F. Würthner
Institut für Organische Chemie
Universität Würzburg
Am Hubland, 97074 Würzburg, Germany
The ORCID identification number(s) for the author(s) of this article can be found under https://doi.org/10.1002/adma.202104678.

DOI: 10.1002/adma.202104678

ambiguous and imprecise definitions of J-aggregates hinder a systematic study of the relationship between aggregation and optoelectronic device properties. Accordingly, after the introduction, the second section of this review article will instruct the reader with new insights into the interpretation of hypso- and bathochromic shifts as well as changes in the band shapes and vibronic progressions in dye aggregates that are quite useful to gather information on both structural and functional properties of aggregated materials. These insights are a prerequisite to understand our interpretations of the currently most successful nonfullerene acceptors (NFAs) in BHJ organic solar cells and narrowband absorbing materials in organic photodiodes, which will be discussed in the following sections.

It is remarkable that the application of J-aggregates in these two important contemporary research fields indeed relates to the first application of J-aggregates as sensitizers in photography. Here, panchromatic absorbers were required for black/white photography while J-aggregates with narrow bands were necessary to distinguish blue, green, and red light. These demands perfectly match the requirements for default OSCs and OPDs, respectively. Accordingly, in the following we will provide a brief introduction to the historic importance of J-aggregates that is interwoven with their application as sensitizers for silver halide grains in photography. While the discovery of J-aggregate formation upon self-assembly of pseudoisocyanine **Cy1 (PIC)** (**Figure 1**a) in water in 1936 by Jelley[17] and Scheibe[18] has been emphasized in many articles, it is not a common knowledge that cyanine dyes were already applied soon after the discovery of Vogel in 1873 as spectral sensitizers for visible light in silver halide photography.[19,20] While panchromatic sensitization was beneficial for black/white photography, later on narrowband sensitizers allowed to distinguish blue, green, and red light in color photography. This goal was accomplished already in the 1930s with cyanine dyes that self-assemble as densely packed 2D J-aggregate monolayers on silver halide grains.[21] Figure 1a shows common sensitizers (**Cy2–4**) for the spectral sensitization of blue, green, and red light based on mono- and trimethine cyanines.[22] Along the same line, J-aggregates of pentamethine cyanine dyes such as **Cy5** were developed as sensitizers for NIR light.[20] In Figure 1b, the concentration-dependent UV-vis absorption of trimethine dye **Cy6 (TDBC)**[23,24] is shown, demonstrating the dependence of the degree of aggregation (α_{Agg}) on the concentration according to a cooperative self-assembly model.[25,26]

Due to the pronounced interest in the spectral sensitization of J-aggregates, other properties of these cyanine dye-based J-aggregates did not receive the same attention or were only brushed over within a small community of researchers during almost one century up into the modern times. One obvious feature of dye aggregates relates to their formation by self-assembly in solution (Figure 1b)[17,18,24] that constitutes an early example of supramolecular polymerization, leading to solutions of high viscosity and hydrogels.[27] Another feature is the increase of fluorescence upon aggregation, a property that has received considerable interest over the last two decades and is now commonly termed aggregation-induced emission (AIE).[28,29] This functional property was already noted by Scheibe in 1937 for J-aggregated **Cy1 (PIC)** dyes[18] and later on observed for a broad variety of other cyanine dyes as described in a recent review

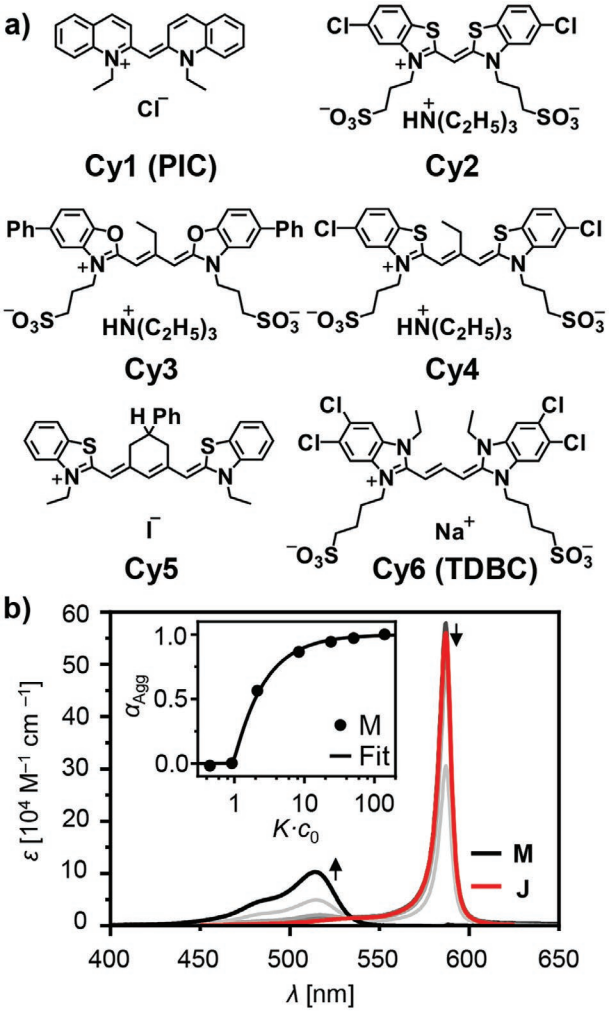

Figure 1. a) Sensitizers for silver halide grains. Surface-bound J-aggregates of monomethine dye **Cy2** act as a sensitizer for blue light, those of trimethine dyes **Cy3** and **Cy4** as sensitizers for green and red light, respectively, and those of pentamethine dye **Cy5** for NIR light at 750 nm. b) Concentration-dependent UV-vis absorption (gray scale) of another common but better soluble spectral sensitizer for green light, 5,5′,6,6′-tetrachloro-1,1′-diethyl-3,3′-bis(4-sulfobutyl)-benzimidazolocarbocyanine **Cy6 (TDBC)**, measured in dilute NaOH alkaline aqueous solution (pH = 11) according to refs. [23,24] alongside the determined monomeric (M; black) and aggregate (J; red) spectra from global fit analysis. The inset shows the degree of aggregation as a function of $K{\cdot}c_0$ according to a K_2–K cooperative self-assembly model[25,26] at a wavelength of 514 nm.

by Demchenko and co-workers.[30] This type of AIE (or more accurately AIEE for aggregation-induced enhanced emission)[31] exemplified by J-aggregates indeed originates from both a decrease of the nonradiative decay rate due to dye rigidification in the aggregate state and an increase of the radiative decay rate due to the redistribution of oscillator strength in the coherently coupled dye aggregate to a strongly allowed lowest exciton state. Accordingly, AIEE and band narrowing are interrelated for cyanine J-aggregates and responsible for the phenomena of superradiance (enhanced emission due to faster radiative decay) and coherent energy transfer within J-aggregates that have been investigated in many laboratories over the last 50 years.[12,32]

2. Packing-Dependent Optical Properties of Dye Aggregates

In this section, we want to make the reader familiar with the different types of J-aggregates and point out that neither a bathochromic shift compared to the absorption spectrum of the monomer nor a slip-stacked packing arrangement in the aggregated state is a sufficient criterion to call an aggregate a J-aggregate. Indeed, a lot of recent literature is erroneous in this regard and sometimes even the red-shifted emission of excimers is mistaken as evidence for a J-aggregate. However, while excimers with their large Stokes shifts and the retarded fluorescence decay compared to the monomeric species are fundamentally different from J-aggregates (small Stokes shift, accelerated fluorescence decay), the term J-aggregate has indeed been continuously broadened over the years (**Figure 2**).

The archetype example for a conventional J-aggregate **Cy1** (**PIC**) as discovered by Jelley[17] and Scheibe[18] is illustrated in Figure 2a. In this type of aggregate, the dyes are organized parallelly in a slip-stacked arrangement (either 1D chain or 2D brickwork) with a slip angle of $\Theta < 54.7°$ in the framework of the simple point-dipole approximation, i.e., Kasha's molecular exciton model.[33] For dyes with the $S_0 \rightarrow S_1$ transition dipole moment (μ_{eg}) polarized along the aggregate axis, only the lowest exciton state originating from a negative Coulomb coupling ($J_{Coulomb}$; also called long-range coupling) is allowed. This leads to the special situation encountered for classical Scheibe- or J-aggregates for dyes with a large μ_{eg}: A narrow absorption band with a strongly increased absorption coefficient, pronounced bathochromic shift (typically ≈ 100 nm), and reduced vibronic fine structure compared to the monomer (Figure 2a). Likewise, a narrow fluorescence band with small Stokes shift and shorter fluorescence lifetime is a typical signature of these aggregates, often accompanied by an increased fluorescence quantum yield. Many cyanine dye aggregates fulfill these spectroscopic criteria,[30] that also ensure other interesting properties such as the presence of delocalized exciton states over a larger number of dyes and efficient exciton migration along the aggregate chain.[32] However, it is noteworthy that the supramolecular structure of many cyanine dye aggregates is not well described by just a simple aggregate chain and that any form of displacement such as deviation from coplanarity will lead to a significant oscillator strength also for higher exciton states.[34,35]

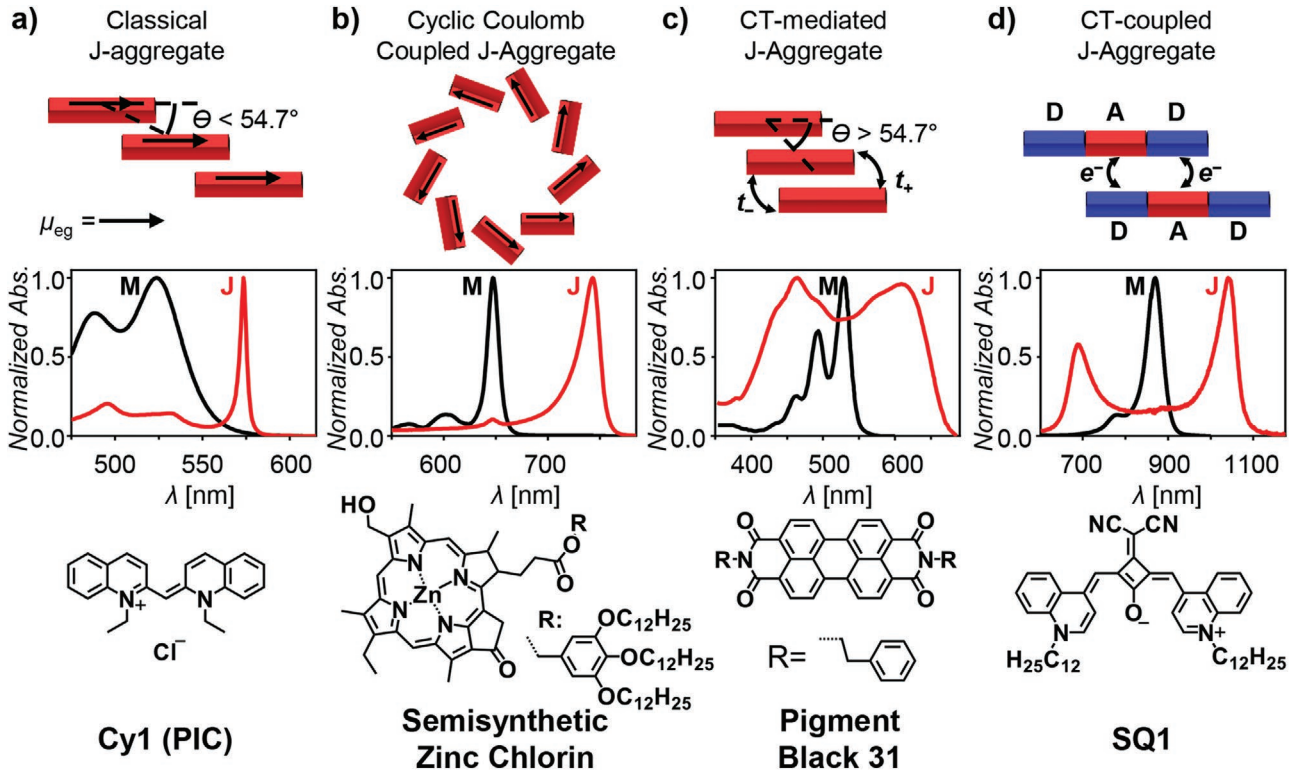

Figure 2. Classification of J-aggregates based on their structural properties in terms of the Coulomb coupling ($J_{Coulomb}$) between transition dipole moments (μ_{eg}; single arrow indicating the oscillation phase for J-type $J_{Coulomb}$) and short-range coupling involving molecular orbitals: a) Classical J-aggregate with a strong $J_{Coulomb}$ and most oscillator strength accumulated in the lowest Frenkel exciton state. b) J-aggregate as found in natural light harvesting systems with a strong $J_{Coulomb}$ but most oscillator strength accumulated not in the lowest Frenkel exciton state but in other low energy states (i.e., negative coupling) of the exciton band. Adapted with permission.[40] Copyright 2008, Wiley-VCH. c) Charge transfer (CT)-mediated J-aggregate with weak J- or H-type $J_{Coulomb}$ whose red-shifted absorption band originates from a wavefunction overlap of closely stacked dyes with a strong negative CT-mediated HOMO–HOMO and/or LUMO–LUMO coupling. Adapted with permission.[47] Copyright 2002, American Chemical Society. d) CT-coupled J-aggregate based on D-A-D dyes with pronounced donor–acceptor interaction leading to the mixing between intermolecular CT and Frenkel states to afford both a hypsochromically and a bathochromically shifted absorption band. Adapted with permission.[49] Copyright 2021, Wiley-VCH. The spectra indicated by black and red lines refer to the monomer (M) and aggregate/solid-state spectra (J) of the corresponding chromophores, respectively.

Over the years after Jelley's and Scheibe's seminal discovery, also other dye aggregates were named J-aggregates despite the fact that in particular their fluorescence properties did not match those of pristine J-aggregates and also band narrowing was often not observed. Among these dye aggregates are those of chlorophyll and bacteriochlorophyll dyes that are found in the light-harvesting antenna complexes of photosynthetic bacteria.[32,36] These dyes are also aggregated in a slip-stacked fashion, however, in cyclic (purple bacteria)[37] or tubular (green bacteria)[38] structures. For this topology and in dependence on the direction of their μ_{eg}, the lowest exciton state is not the one with the largest oscillator strength.[39] Nevertheless, within the exciton band originating from the larger dye manifold, states originating from negative coupling still dominate the allowed optical transitions, thereby leading to a pronounced bathochromic shift of the absorption band such as for the semisynthetic zinc chlorin derivative shown in Figure 2b.[40] Thus, despite a pronounced bathochromic shift and increased absorption coefficients for the J-bands, the fluorescence decay rate and quantum yields are decreased compared to those of the monomers. Because the absorption and fluorescence properties of these dye aggregates are still understandable based on long-range $J_{Coulomb}$, it appears reasonable to also call them J-aggregates. Because natural evolution has optimized this type of dye aggregate for efficient sun light harvesting and transfer of excitation energy to reaction centers, the organizational principles of these aggregates (cycles, tubes) might be a blueprint for organic photovoltaic materials, as they exhibit exceptional long-range energy transport which is beneficial for such devices as generated excitons can thus more easily reach a required interface.[32]

However, red-shifted absorption bands are not necessarily a signature of a gain in oscillator strength for exciton states characterized by a negative, i.e., J-type long-range $J_{Coulomb}$. Instead, red-shifted absorption bands may also arise from short-range charge transfer (CT)-mediated coupling for dyes with pronounced wave function overlap as in the case of π-stacked chromophores.[41] Accordingly, a significant highest occupied molecular orbital (HOMO) overlap, i.e. HOMO–HOMO and lowest unoccupied molecular orbital (LUMO) overlap, i.e. LUMO–LUMO can, depending on the sign of the electron and hole transfer integrals, result in J-type short-range coupling which may compensate (leading to a "null-aggregate")[42,43] or even outmatch an H-type $J_{Coulomb}$ (Figure 2c).[44] Indeed, while a longitudinal displacement of ≈ 7 Å is required for a negative Coulomb coupling for the important class of perylene bisimide (PBI) dyes,[45,46] it was shown that a longitudinal displacement of only ≈ 3 Å provides a very large negative CT-mediated coupling that counteracts the minor positive $J_{Coulomb}$, thereby leading to a two-band absorption spectrum with a J-aggregate-like bathochromically shifted band as well as an absorption band at shorter wavelengths.[45,46] Such strong J-type short range coupling is indeed responsible for the panchromatic absorption feature of PBI dye Pigment Black 31 in the solid state, which shows a red-shifted absorption band despite the presence of pronounced H-type $J_{Coulomb}$ (Figure 2c).[47]

A similar two-band absorption spectrum with a bathochromically shifted band at longer wavelengths can be observed for aggregates based on donor–acceptor–donor (D-A-D) chromophores such as squaraine **SQ1** with H-type $J_{Coulomb}$ and pronounced donor–acceptor interaction between the monomers (Figure 2d) due to a significant HOMO–LUMO overlap. For this situation, energetically low-lying CT states mix with Frenkel states, leading to optically allowed states at both higher and lower energy compared to the monomer. This often affords panchromatic absorption spectra as observed for many squaraine dyes in the solid state[48,49] as well as for aggregates in solution.[48,50] Hence, a red-shift of the absorption band is present even though the chromophore arrangement may induce H-type $J_{Coulomb}$. We would like to emphasize that the energetic separation between the two absorption bands in the aggregate spectrum, i.e., the batho and hypsochromic shift, is not due to Davidov splitting but reflects the strength of the donor–acceptor interaction. For the most suitable theoretical treatment for the respective classes of dyes, we refer the reader to recent articles by Spano and co-workers.[41,42,48] In the following, we will denote all aggregates whose bathochromic shift mainly arises from short-range coupling associated with wavefunction overlap (Figure 2c,d) as CT-J-aggregates.

Consequently, the above-mentioned examples illustrate that the observation of a red-shifted absorption band does not necessarily prove the presence of J-type aggregates as defined within the conventional exciton theory, i.e., a slip-stacked chromophore arrangement with a large longitudinal displacement ($\Theta < 54.7°$) demonstrating significant excitonic coupling. Especially in the case of π-stacked chromophores, additional short-range interactions come into play, which can lead to the observation of a red-shifted absorption band even though an H-type or negligible $J_{Coulomb}$ is present. Indeed, a red-shift of the absorption band upon aggregation can also occur due to polarizability effects, which overcompensates the blue shift arising from H-type $J_{Coulomb}$. Such bathochromic shifts despite weak H-type coupling have been observed for polarizable squaraine[51] and carotenoid dye aggregates[52] arising from a gas-to-crystal shift that surpasses the blue-shift caused by $J_{Coulomb}$ due to a larger stabilization of the more polarizable excited state compared to the ground state upon aggregation. Hence, the classification of a J-aggregate solely based on the observed red-shift can be misleading. Instead, the change of the vibronic pattern, i.e., an increase of the ratio of the intensities of the 0–0 and 0–1 bands can often be used as a reliable criterion for the classification of a classic J-aggregate.[53]

3. Organic Solar Cells

With an increasing concern about global warming, the sustainable harvesting of sunlight by OSCs has drawn a considerable amount of research interest over the past three decades. Compared to their inorganic counterparts, OSCs exhibit advantages like device flexibility, semitransparency, light weight, and the possibility to chemically tailor their functional properties.[54–56] Particularly, recent development of crystalline NFAs containing slip-stacked molecular packing pushed the power conversion efficiency (*PCE*) of OSCs above 18%.[57,15] As discussed in the previous section, the slip-stacked arrangement promotes unique excitonic and electronic characteristics, which directly affect the OSC performance. Therefore, understanding the

interdependence between the supramolecular structure and the physical processes in such devices is essential for developing high-performing OSCs.[10,15]

The *PCE* as the central figure of merit for OSCs is directly proportional to the short-circuit current density (J_{sc}), the open-circuit voltage (V_{oc}), and the fill factor (*FF*) of the device:

$$PCE = \frac{J_{SC}\ V_{OC}\ FF}{P_{Light}} \quad (1)$$

where P_{Light} is the optical power. Accordingly, the *PCE* is highly dependent on the absorption spectra, energetic levels, charge carrier mobilities, and morphology within a device's active layer(s).[58] To achieve a high J_{sc}, a broad absorption band is required from the active layer materials to convert as many incident photons as possible into excitons, which migrate to the donor–acceptor interface for charge separation and are finally extracted after charge transport to the electrode as free charge carriers. As such, a classic Coulomb-coupled J-aggregate as described by Kasha's theory (see Section 2) with an exchange-narrowed absorption band is not suitable for the application in OSCs for solar light harvesting. It is worth noting, however, that while such OSCs by default demand panchromatic absorption spectra for the generation of large photocurrents, in recent years especially visible transparent OSCs have received a large research interest as showcased in review articles on the topic.[56,59,60] For wavelength-selectivity in such semitransparent devices, an NIR-shifted absorption feature through $J_{Coulomb}$ J-type aggregation is of high interest. These devices therefore have a large similarity with visible-transparent OPDs which will be discussed in Section 4. However, for conventional OSCs for panchromatic solar light harvesting a mixture of different J-type interactions (vide infra) through increased and extended π-overlap in the slip-stacked arrangement as illustrated in Figure 2c helps retaining intense and broad absorption features and therefore appears more promising. Here, it is worth noting that 2D brickstone-type π-stacking arrangements are also beneficial for a more isotropic charge carrier transport compared to 1D π-stacks.[61] The voltage loss and corresponding V_{oc}, which are currently being discussed as a key issue within the OSC community, do not only depend on the energy levels of the individual donor and acceptor in the BHJ thin film, but also on the nature of the CT states and the morphology at the donor–acceptor interface.[62]

In the following sections, the impact of the state of aggregation in the solid state on OSC device performance is discussed for representative organic semiconductor molecules. In literature, aggregation effects in OSCs have been reported for molecules bearing benchmark chromophore backbones including diketopyrrolopyrroles (DPPs),[63,64] boron-dipyrromethenes (BODIPYs),[65,66] perylene dye oligomers (PBIs/PDIs),[67,68] D-A-D,[69,70] and acceptor–donor–acceptor (A-D-A)[71,72] dyes, or even polymers.[73,74] In most cases, however, a lack of sophisticated theoretical investigations and crystallographic data prevents an in-depth understanding of the aggregation mode and its effects on optical properties in solid state and the corresponding device properties. Therefore, in Section 3.1, we focus on D-A-D squaraine donor dyes used in OSCs exhibiting J-type packing as squaraine dyes are not only an important class of donor molecules in OSCs,[75–78] but as their structure–property relationship has also been extensively investigated based on state-of-the-art theoretical methods as well as experimental results. Section 3.2 covers the field of acceptor–donor–acceptor (A-D-A) NFAs bearing 1,1-dicyano-methylene-3-indanone (DCIND) as acceptor moieties which yield the to-date highest performing OSC devices.

3.1. Donor J-Aggregates Based on Donor–Acceptor–Donor (D-A-D) Dyes

D-A-D dyes are typically of electron-rich character and have been widely used as donor components in BHJ solar cells. For the reasons outlined above, in this section we will focus on squaraine dyes which describe a class of molecules consisting of an electron-accepting squaric acid central core substituted with two electron-donating (hetero-)aromatic units at either side. As such, these dyes constitute D-A-D-type organic semiconductors with a high tinctorial strength in the red to NIR spectral region which have been successfully employed in squaraine:fullerene-based OSCs with peculiar aggregation behaviors.[75] Endowed by large π–π and electrostatic interactions, it is common for squaraine dyes to form aggregates[12,79] and accordingly a large variety of supramolecular structures[80] have been reported that exhibit excitonic coupling of H- as well as J-type character depending on the packing arrangement. Already in 2002, Tian et al. could demonstrate how the state of aggregation for squaraines like **SQ2a–d** (**Figure 3**) in thin films can be directed through the sterical demand of substituents at the donor moiety. Derivatives with linear alkyl chains were adopted due to their higher flexibility rather H-type packing motifs through direct face-to-face π-stacking, while sterically more demanding branched alkyl chains directed the dyes into a slip-stacked packing arrangement with J-type coupling,[81] which is according to our current understanding based on Coulomb as well as CT-mediated coupling depending on their molecular arrangement in the solid state.

The first example that pointed at the usefulness of J-type aggregation in such systems for OSCs was provided by our collaborative research with Meerholz and co-workers for

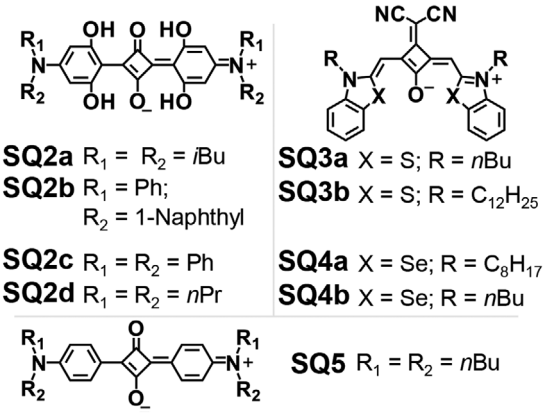

Figure 3. Chemical structures of representative squaraine dyes used in organic electronics and solar cells.

dicyanomethylene acceptor-substituted squaraine dyes in 2009, which showed a pronounced bathochromic shift of more than 100 nm of the absorption maximum in the solid state (822 nm) with respect to the monomer (702 nm) in solution (**Figure 4**a).[82] In this study, the dipolar squaraine dye **SQ3a** (see Figure 3) was employed in solution-processed OSCs in a BHJ device architecture with $PC_{61}BM$ as acceptor yielding a *PCE* of 1.79%. While these devices suffered from a low open-circuit voltage (V_{oc} = 0.31 V), their short-circuit current densities (J_{sc} = 12.6 mA cm^{-2}) were outstanding after annealing into the J-aggregate state. In the aggregated state, **SQ3a** hereby adopts a slip-stacked packing arrangement with a π–π distance ($r_{\pi-\pi}$) of 3.35 Å and a slip angle (Θ) of about 27° as depicted in Figure 4b, which results in a negative $J_{Coulomb}$ of around –2000 cm^{-1} according to Kasha's exciton theory (vide supra). Within this dimer, the two chromophores align in an antiparallel fashion to compensate their permanent ground-state dipole moments (μ_g). Through the additional mismatched overlap of the acceptor and donor moieties of the two π-stacked chromophores, the dimer may exhibit intermolecular as well as intramolecular CT coupling (vide supra), as is common for such D-A-D dyes with a zwitterionic nature and has been convincingly elaborated by Spano and co-workers (vide infra).[48] Recent examples demonstrate how this can lead to very distinct absorption spectra with two sharp absorption bands through CT-mediated J-type coupling (vide infra).[49] In the case of **SQ3a**, this characteristic is only hinted at by an additional shoulder around 660 nm (Figure 4a), but might also arise from a second dimer within its crystal structure, which is rotationally displaced by 87°. In comparison, selenium-containing **SQ4a** adopts a uniform extended J-type packing motif with exclusively slip-stacked neighbors (Θ = 29°) with a very close $r_{\pi-\pi}$ of 3.18 Å (Figure 4c). This leads to a more distinct absorption spectrum in the solid state with a much narrower band shape when compared to **SQ3a** (Figure 4a). Notably, also here a small second absorption feature around 610 nm is observable that might indicate CT-mediated coupling.

For **SQ3a**:$PC_{61}BM$ thin films, these well-packed J-type domains, alongside the resulting bathochromically shifted absorption spectrum into the NIR region, enable a good free charge-carrier transport within an OSC's active layer and lead to high J_{sc} values.[82] A record value at the time, even today this high J_{sc} of 12.6 mA cm^{-2} still compares well to the highest J_{sc} value for squaraine-based OSCs of 15.2 mA cm^{-2} within a ternary BHJ OSC.[83] This exceptional performance of a slip-stacked J-type aggregate in regard to charge carrier mobility is also observable in organic thin-film transistor (OTFT) studies conducted on the structurally similar derivatives **SQ3b** and **SQ4b**, with either longer solubilizing alkyl chains or benzoselenazol donor units, respectively. Both dyes exhibit extended slip-stacked packing arrangements in their crystalline thin films analogous to that shown in Figure 4b, leading to strongly bathochromically shifted absorption spectra. For solution-processed OTFTs of **SQ3b**, this resulted in maximum hole mobilities (μ_h) of 0.08 cm^2 V^{-1} s^{-1}, while vacuum-fabricated devices of selenium-containing dye **SQ4b** exhibited a μ_h of up to 1.3 cm^2 V^{-1} s^{-1},[84] clearly demonstrating the benefit of this highly crystalline and extended slip-stacked packing motif. A

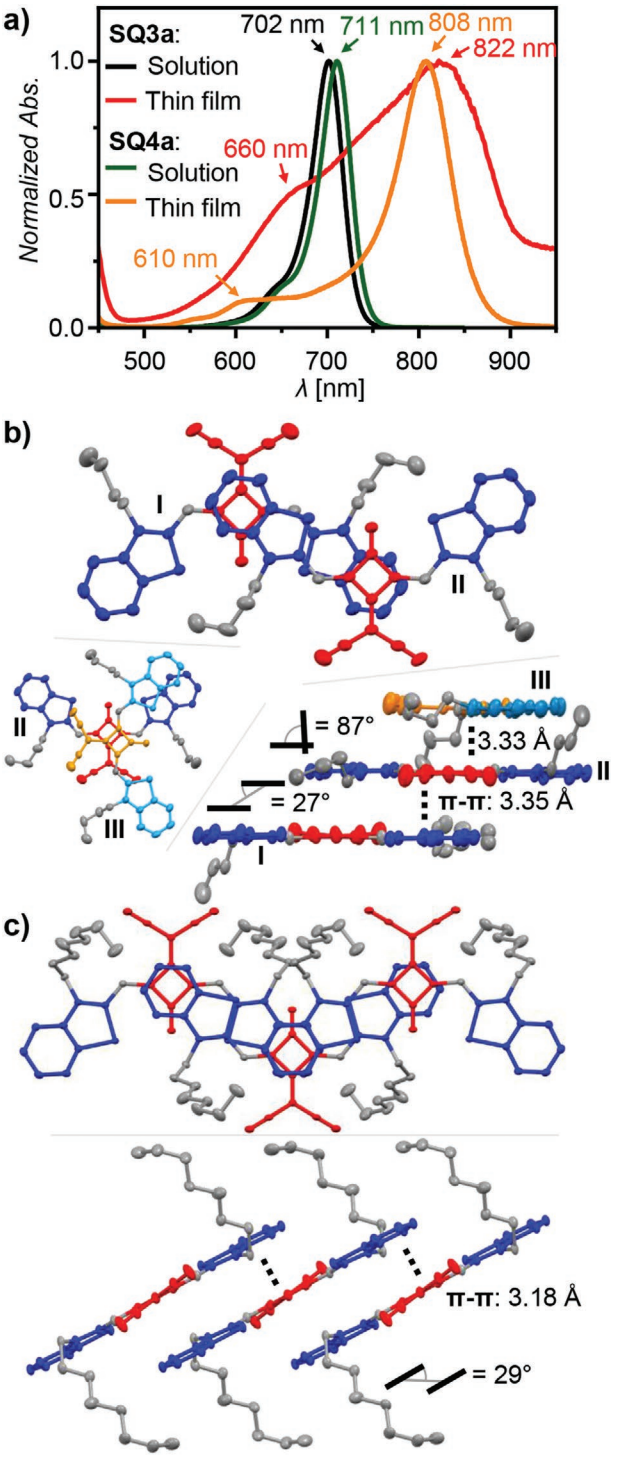

Figure 4. a) Absorption spectra and their maxima of **SQ3a** and **SQ4a** in solution (black/green) and their respective annealed thin films (red/orange). Adapted with permission.[82] Copyright 2009, Wiley-VCH. Adapted with permission.[84] Copyright 2014, American Chemical Society. b,c) The top (top) and side (bottom) view of the single-crystal structure of the two nearest neighbors of **SQ3a** and **SQ4a**. The acceptor and donor moieties are colored red and blue, respectively. Hydrogen atoms have been omitted for clarity and the thermal ellipsoids are set at 50% probability.

Table 1. OSC performance parameters of OSCs with solution-processed squaraine dyes **SQ2–5** as donor materials in combination with solution- ($PC_{61}BM$) or vacuum-deposited (C_{60}) fullerene acceptors.

Donor	Fullerene	Coupling[a)]	Active layer(s)	V_{oc} [V]	J_{sc} [mA cm^{-2}]	*FF* [%]	*PCE* [%]	Ref.
SQ2a	C_{60}	–	PHJ	0.79	8.6	53	3.6	[90]
SQ2b	C_{60}	J	PHJ	0.90	10.0	64	5.7	[90]
SQ2c	C_{60}	J	PHJ	0.94	7.4	72	5.2	[94]
SQ3a	$PC_{61}BM$	J	BHJ	0.31	12.6	47	1.8	[82]
SQ3a	$PC_{61}BM$	A	BHJ	0.37	1.5	30	0.2	[85]
SQ3a	$PC_{61}BM$	H	BHJ	0.47	3.0	43	0.6	[85]
SQ3a	$PC_{61}BM$	J	BHJ	0.30	11.5	48	1.6	[85]
SQ5	C_{60}	H	PHJ	0.25	3.8	50	0.5	[86]
SQ5	C_{60}	J	PHJ	0.52	6.5	53	1.8	[86]

[a)]The respective H- or J-type coupling is based on the according reference and/or tentative according to our judgement. A is for monomer-like, i.e., amorphous.

follow-up study[85] on **SQ3a**-based BHJ OSCs elucidated the impact of different states of aggregation on OSC performance. In dependence on the annealing temperature used for thermal treatment of the active layer with $PC_{61}BM$, the same material **SQ3a** demonstrated amorphous, H-type or J-type coupled states. Going over from an amorphous to an H-type state, J_{sc} increases up to 200% due to the suggested 1D π-stacking. Upon formation of J-type aggregates, the J_{sc} is enhanced even further to over 750% due to the now improved 2D percolation pathways and more favorable exciton transport characteristics. An overview of the OSC performance parameters of squaraine-based OSCs is given in **Table 1**.

For squaraine **SQ5**, Yang and co-workers demonstrated both H- and J-type aggregation according to their optical and X-ray diffraction data in the solid state in dependence on the solvent used for spin-casting.[86] On the one hand, the use of the high boiling solvent *ortho*-dichlorobenzene (*o*DCB) led to the formation of a thermodynamically stable H-type aggregated state as suggested through hypsochromically shifted and narrowed absorption band. On the other hand, the use of low boiling solvents such as dichloromethane favored a kinetically self-assembled meta-stable J-type aggregation state[87] as suggested by a red-shifted absorption band. Hereby it is worth noting that due to a large distance between parallely oriented **SQ5** chromophores in the single crystal (9.44 Å) and a Θ of 53° close to the magic angle,[88] the resultant $J_{Coulomb}$ is negligible while a mismatched overlap of the donor and acceptor units resulting in possible CT-mediated coupling may explain the observed dual-band absorption feature within the aggregate film. Planar heterojunction (PHJ) OSCs with active layers of H- or J-type coupled **SQ5** and C_{60} showed an increase in *PCE* from 0.5% to 1.8%, respectively, again coinciding with an increase in J_{sc} from 3.8 to 6.5 mA cm^{-2} due to improved NIR absorption and the more 2D percolation pathways of the presumably slip-stacked J-aggregates.

Related research by Thompson and co-workers[89] on **SQ2a–c** suggested that a change of the substituents of such a centrosymmetric linear squaraine dye from sterically demanding alkyl (**SQ2a**) chains to rigid aryl substituents (**SQ2b–c**) at the donor position may enhance the molecular packing capability in the solid state with induction of a slip-stacked packing arrangement. 1-Naphthyl/phenyl substituted derivative **SQ2b** indeed confirmed this hypothesis through an increased OSC performance reaching a *PCE* of 5.7% as opposed to 3.6% for **SQ2a** in combination with vacuum-deposited C_{60}.[90] Notably, the change in donor material improved the J_{sc} from 8.6 up to 10.0 mA cm^{-2} and the *FF* from 64% to even 72% within the same optimized PHJ device architecture. This value for squaraine-based OSC is indeed only exceeded by vacuum-fabricated BHJ devices or tandem OSCs achieving 6.3%[91] and 8.3%,[92] respectively.

While unfortunately no single-crystal structure of **SQ2b** is available, its analogous squaraine **SQ2c** adopts a slip-stacked packing arrangement ($r_{\pi-\pi}$ = 3.34–3.61 Å; Θ = 34°–39°; $J_{Coulomb} < 0$ cm^{-1}) with a mismatched overlap of donor and acceptor analogous to **SQ3a**.[93] Similar to its congener, **SQ2c** is also able to reach a *PCE* of 5.2% through a high charge-carrier mobility indicated by an *FF* of 72%.[94] The rationale for the success of such squaraines might accordingly be the combination of a slip-stacked packing arrangement facilitating J-type $J_{Coulomb}$ in addition to an intermolecular overlap of donor and acceptor moieties enabling CT-mediated coupling as discussed by Spano for analogue dye **SQ2d**.[42] As shown in **Figure 5**, **SQ2d** exhibits a two-band absorption feature in the solid state, which is attributable to CT-mediated coupling of neighboring chromophores in addition to $J_{Coulomb}$.

A quite general observation is an increase of both J_{sc} and *FF* for the slip-stacked J-type coupled materials described above, presumably originating from the concerted effect of a highly red-shifted absorption band, longer exciton diffusion length as well as improved 2D percolation pathways in contrast to the 1D card-stack like arrangement of H-type coupled systems. What is however still puzzling concerning the OSC performance of molecular aggregates is the fact that the V_{oc} shows no clear trend in dependence on the molecular aggregate. For instance, while for **SQ5**-based devices a change in V_{oc} from 0.25 to 0.52 V is observed upon going over from the H- to J-type aggregation, this trend is reversed for **SQ3a** with 0.47 V (H) to 0.30 V (J) (Table 1). Yang and co-workers suggest this change for **SQ5** is dependent on a deepening of the ionization potential due to CT interactions within the J-type aggregates,[86] while Forrest and co-workers suggested the increase in V_{oc} to 0.90 V in J-type aggregating **SQ2b** compared to 0.79 V for **SQ2a** occurs through a reduced HOMO level due to the reduced electron-donating

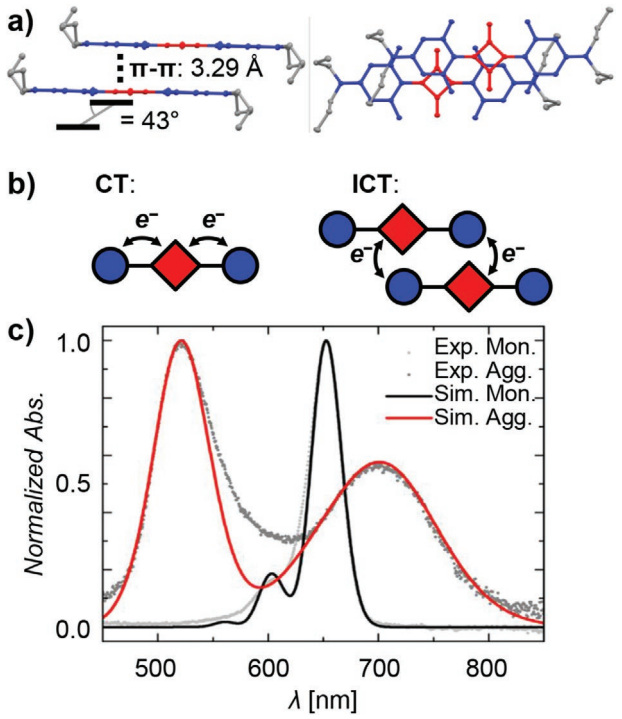

Figure 5. a) Side (left) and top (right) view of the single-crystal structure of **SQ2d**. b) Schematic depiction of intra- and intermolecular CT coupling in squaraine dyes. c) Simulated (solid) and experimental (gray) spectra of **SQ2d** as monomer (black) and aggregate (red) in solution. b,c) Adapted with permission.[48] Copyright 2015, American Chemical Society.

character of the arylamine compared to the alkylamine end-groups.[90] As such the effect of the state of aggregation on V_{oc} is an aspect of the OSC performance which definitely needs further in-depth investigation in the future. Still, even here, the differentiation between optical (absorbance, J_{sc}), energetic (loss factor, V_{oc}), and morphological (exciton migration, charge transport, *FF*) aspects detrimental to the device performance will be difficult to quantify and to distinguish, as the entire device architecture including all interfaces to and within the active layer is important. In this aspect, it is worth to pay attention to a recent study by Vandewal and co-workers, who used a strong light–matter coupling effect to induce a red-shifted polariton absorption band. Despite a lower driving force for charge separation, such devices exhibit a similar V_{oc} to non-coupled devices.[95] This suggests that V_{oc} is not only derived from a change in local transition energy, which in turn highlights the dependence of V_{oc} of aggregation-based devices from film morphology and intermolecular CT states.

3.2. Acceptor J-Aggregates Based on Acceptor–Donor–Acceptor (A-D-A) Dyes

The highly successful development of A-D-A dyes as NFAs was a true game changer in the field of polymer-based OSC resulting in record *PCE* values.[96,97] Accordingly, beyond favorable molecular properties (i.e., intense absorption bands up to the NIR spectral range, tunable LUMO levels), the amazing success of A-D-A dyes may also be attributed to their state of aggregation.[98] Because all highly successful A-D-A dyes contain a DCIND acceptor unit connected via a methine bridge to a thiophene of the central donor unit, it is instructive to take a look onto some earlier reported dipolar D-A dyes, which were used successfully as donor materials in combination with fullerenes in OSCs in both solution as well as vacuum-fabricated devices.[99–101] Thus, merocyanines **MC1-2** (see **Figure 6**) represent the first small molecules bearing a DCIND

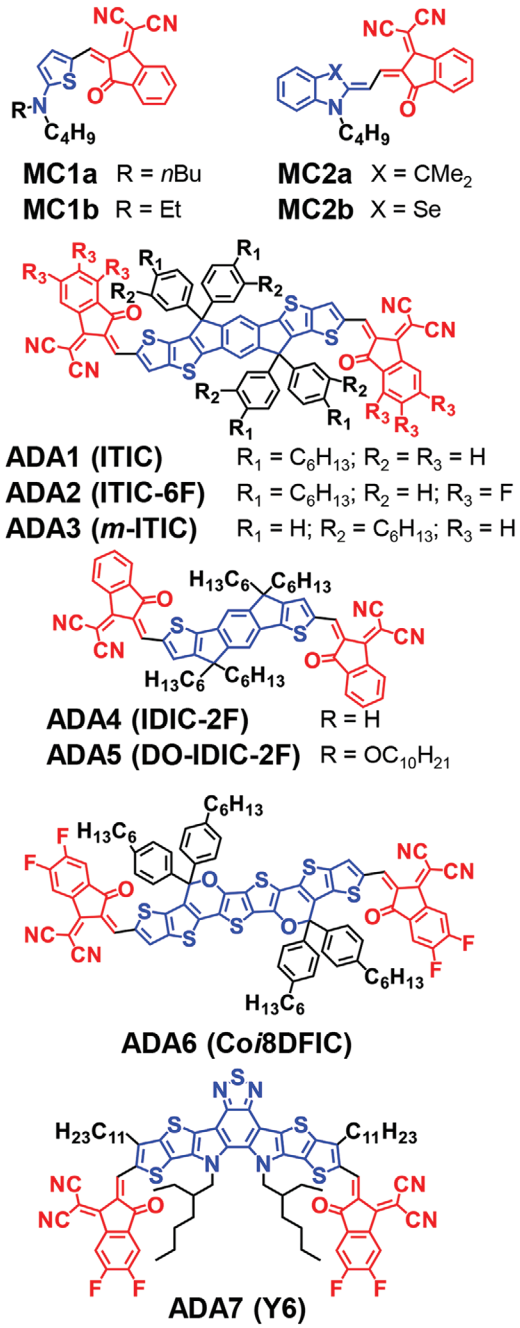

Figure 6. Chemical structures of representative merocyanine D-A dyes utilized as electron donors and A-D-A-type NFAs. The donor and DCIND-based acceptor moieties are highlighted in blue and red, respectively.

moiety used in OPV. In particular, as shown by the groups of Meerholz and Würthner, **MC1a** shows the planarity-enforcing S···O chalcogen-bonding interaction between the thiophene's sulfur and the acceptor heterocycle's carbonyl group[102] as well as an antiparallel arrangement of neighboring molecules in the solid state by strong dipole–dipole interactions[4] as depicted in **Figure 7**a–c. Because these features are omnipresent in virtually all high-performing A-D-A dyes (vide infra), **MC1a** and **MC1b** may be considered as their progenitor in terms of molecular and supramolecular design despite the fact that they were utilized as donor components. When introduced in 2011, the accomplished *PCE* of 4.5% in a simple solution-processed BHJ device architecture of **MC1b** with $PC_{71}BM$ constituted indeed a record value at the time.[100] Due to the dimer-pairing being the dominating contributor in the aggregation of **MC1a**, no extended well-defined aggregate domains are formed, yielding a broad absorption spectrum (Figure 7d).[103] Indeed, for such dipolar merocyanine dyes, it is not easy to accomplish the desired optical properties by packing control for OSCs. Either antiparallel dimers remain inhomogenously packed with desirable broad absorption bands but a reduced charge carriers mobility or they are prone for self-assembly into extended 1D card-stack arrangements with pronounced Coulomb H-coupling as shown for bis-merocyanine **Bis-MC1** (Figure 7e,f).[104] Going over from its monomeric (open, 536 nm) to its H-coupled dimeric (folded, 513 nm) state, **Bis-MC1** continues to form extended card-stacked H-aggregates in the solid state, yielding over 100 nm hypsochromically shifted (414 nm) and exchange narrowed absorption band. Very high photocurrents were shown for this band but due to the narrow band and location at the blue edge of the solar spectrum, such Coulomb-coupled dye aggregates are not suitable for high-performing OSCs.

In a follow-up study, merocyanines **MC2a** and **MC2b**, which exhibit structure-dependent packing motifs, were investigated.[101] A derivative of **MC2a** bearing an indandione acceptor moiety formed isolated and centrosymmetric dimers in the solid state, leading to low *PCE* values of only 1.0%. A replacement of the indandione with a DCIND moiety for **MC2a** and **MC2b** successively increased the ground state dipole moment and induced extended π-stacking leading to H- and J-type aggregation with a Θ of ≈ 90° and 49°, respectively. This increased the *PCE* up to 3.4% for the 1D antiparallelly aligned H-type coupled π-stacks of **MC2a** and up to even 5.2% for the J-type aggregating **MC2b** demonstrating a staircase-like herringbone structure. The DCIND moiety hereby plays an essential role for this improved device performance. Due to its highly electron-withdrawing character, the DCIND group leads to pronounced intramolecular electronic interactions between the acceptor and donor moieties, effectively increasing both conjugation and dipolarity of the molecule, as well as to a lowering of the LUMO level, yielding bathochromically shifted absorption spectra. Alongside a higher tinctorial strength resulting from an increase in μ_{eg}, this is beneficial for achieving higher J_{sc} values in an OSC. It has also been shown that end-capping of acceptor units with cyano groups reduces the energy loss in OSCs due to the beneficial effect on the energetic landscape within the active layer.[105,106]

From a supramolecular perspective, the DCIND group supports a rigid π-system framework as for **MC1** and **MC2** dyes by

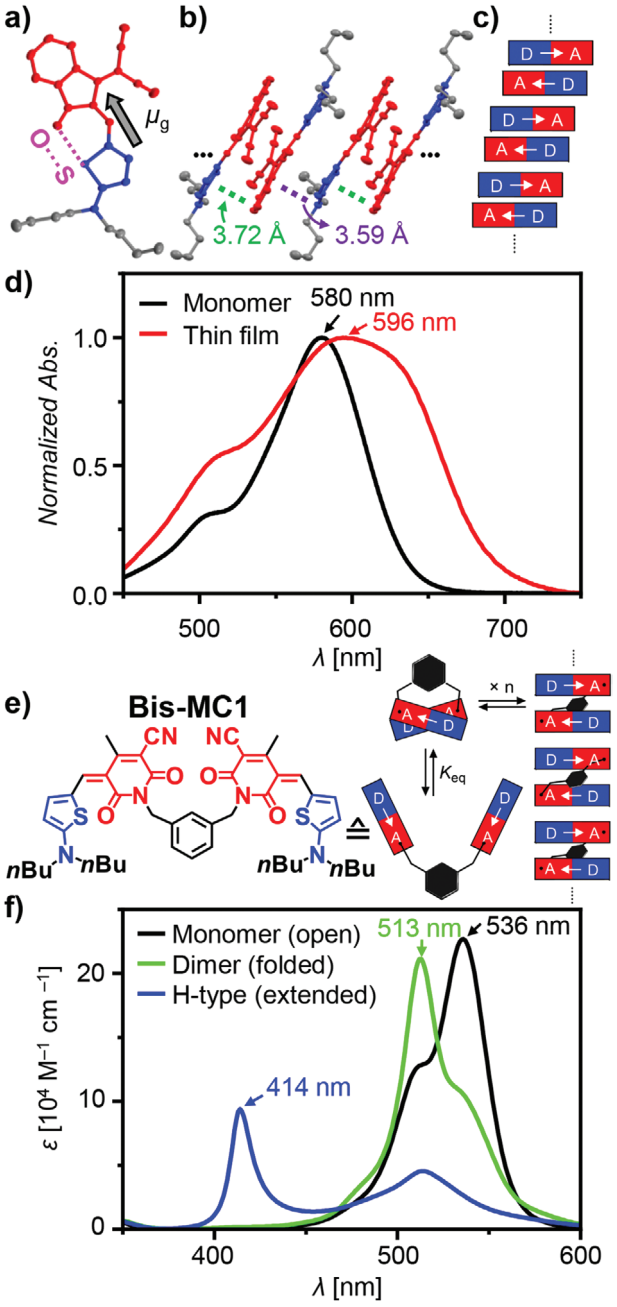

Figure 7. a) Molecular structure of **MC1a** in the single crystal with the O···S chalcogen bond and the direction of the permanent dipole moment μ_g highlighted. b,c) The packing motif in the single-crystal structure and a schematic depiction of extended, antiparallelly aligned **MC1a** π-stacks, respectively. Hydrogen atoms have been omitted for clarity and the thermal ellipsoids are set at 50% probability. d) Solution and thin film absorption spectra of **MC1a**. Adapted with permission.[103] Copyright 2014, American Chemical Society. e) Molecular structure of **Bis-MC1** and its associated concept for the hierarchical supramolecular polymerization into extended cofacially stacked H-type aggregates. f) UV-vis absorption spectra of **Bis-MC1** in its open/monomeric (black), folded/dimer (green), and extended H-type aggregate (blue) structure recorded in mixed tetrahydrofuran-methylcyclohexane solution. e,f) Adapted with permission.[104] Copyright 2013, the Royal Society of Chemistry. All acceptor and donor moieties are colored red and blue, respectively.

Table 2. OSC performance parameters of highlighted A-D-A-based OSCs.

A-D-A NFA	Donor	V_{oc} [V]	J_{sc} [mA cm^{-2}]	*FF* [%]	PCE_{max} [%]	Ref.
ADA1 (ITIC)	**PTB7-Th**	0.81	14.2	59.1	6.8	110]
ADA1 (ITIC)	**PBDB-TF**[a)]	1.00	14.8	56.5	8.7	[111]
ADA1 (ITIC)	**PBDB-T**	0.90	18.7	65.3	10.9	[115]
ADA2 (ITIC-6F)	**PBDB-TF**[a)]	0.81	21.2	66.7	11.9	[111]
ADA1 (ITIC)	**J61**	0.90	17.7	64.6	10.6	[116]
ADA3 (*m*-ITIC)	**J61**	0.90	18.3	69.6	11.8	[116]
ADA4 (IDIC-2F)	**PBDB-TF**[a)]	0.85	18.0	75.8	11.5	[117]
ADA5 (DO-IDIC-2F)	**PBDB-TF**[a)]	0.86	19.6	76.5	13.0	[117]
ADA6 (CO*i*8DFIC)	**PTB7-Th**	0.70	19.9	65.0	9.3	[119]
ADA6 (CO*i*8DFIC)	**PTB7-Th**	0.69	27.3	71.0	13.8	[119]
ADA7 (Y6)	**PBDB-TF**[a)]	0.82	25.2	76.1	15.7	[120]
ADA7 (Y6)	**D18**	0.86	27.7	76.6	18.2	[57]

[a)]Also denoted as PM6 in the literature.

S···O or CH···O noncovalent interactions, respectively.[107] Additional supramolecular aspects were manifested first for D-A dyes and later on also in A-D-A dyes. As such, the dipolarity encoded in the thiophene-methine-DCIND subunit provides a strong structure-directing supramolecular synthon[4,108] that may be responsible not only for the slip-stacked packing motif observed in many NFAs but also for the special porosity-enabling motif seen in crystals of **ADA7 (Y6)** (vide infra). Chalcogen bonding is commonly observed in A-D-A dyes between thiophene rings adjacent to the acceptor building blocks, thereby affording oxygen–sulfur conformational locks.[100,102,109] Accordingly, molecular and supramolecular features first observed for D-A dyes proved to be highly relevant for the design of A-D-A dyes that exhibit excellent charge carrier and exciton transport as well as broadband absorption properties due to an ideal packing arrangement for the application in OSCs.

A main representative of centrosymmetric A-D-A dyes is the indacenodithienothiophene derivative **ADA1 (ITIC)**. This dye was first described by Zhan and co-workers in 2015 and successfully employed in BHJ OSCs with a maximum *PCE* of 6.8% as a nonfullerene electron acceptor with the polymeric donor **PTB7-Th** (for details on OSC performance parameters see **Table 2**).[110] In its single-crystal structure, **ADA1 (ITIC)** exhibits two distinct dimer pairs I–II ($r_{\pi-\pi}$ = 3.35 Å; r_{μ} = 19.4 Å; Θ = 9°; α = 25°) and I–III ($r_{\pi-\pi}$ = 3.41 Å; r_{μ} = 24.0 Å; Θ = 10°; α = 25°) (**Figure 8**a) which according to our analysis exhibit $J_{Coulomb}$ coupling values of −300 and −150 cm^{-1}, respectively. The bulky solubilizing substituents at the central donor moiety direct a slip-stacked packing arrangement with small slip angles which result in negative $J_{Coulomb}$. Despite the large distance (r_{μ}), Coulomb coupling amounts to several hundred wavenumbers due to the huge μ_{eg} (14.4 D). **ADA1 (ITIC)** also retains a very planar conformation in the solid state again supported by conformational oxygen–sulfur locks.[111] The huge longitudinal displacement with slip angles of 8–11° of the end-group stacked chromophores is introduced by the four bulky phenyl–hexyl substituents, which additionally ensure outstanding solubility for highly concentrated blend solutions. The π-stacking mimics the aforementioned antiparallel alignment of the (partial) ground-state dipole moments as discussed for **MC2a** (vide supra). In this packing structure, **ADA1 (ITIC)** exhibits rather isotropic electron transfer integrals ranging from 3.9 to 11.4 meV and forms an extended 2D percolation network, making it an especially promising candidate for BHJs with a high tortuosity, so a high ratio between the path length

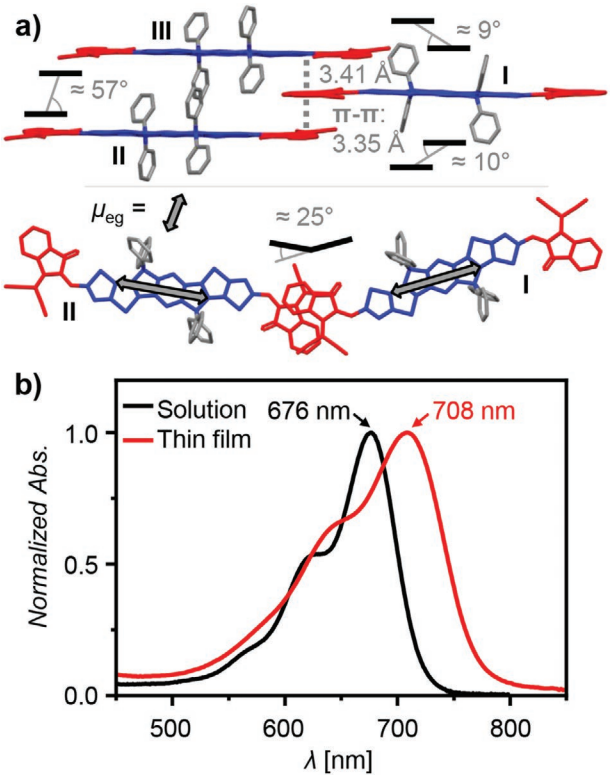

Figure 8. a) Side (top) and top (bottom) view onto the packing arrangement in the **ADA1 (ITIC)** single-crystal structure according to ref. [111]. The two-headed arrows mark the respective 14.4 D strong transition dipole moment (μ_{eg}) axis of each chromophore. Alkyl chains and hydrogen atoms have been omitted for clarity. b) Solution (black) and thin-film (red) absorption spectra of **ADA1 (ITIC)**.

for a charge carrier through the BHJ and an ideal straight path to the respective electrode.[112,113] Going over from the molecular solution to the aggregated solid state, the absorption spectrum of **ADA1 (ITIC)** shows only a modest red-shift of about 32 nm (669 cm^{-1}) along with spectral broadening (Figure 8b). This is in line with the small $J_{Coulomb}$ derived from the simple point-dipole moment approximation of the Kasha theory. The rather broadened absorption spectrum in the solid state might also be influenced by additional intermolecular interactions due to close π-contacts with some degree of CT coupling (Figure 8a). As such **ADA1** (**ITIC**) retains the benefits of slip-stacked J-aggregates as demonstrated by its large exciton diffusion length of 25–32 nm[114] without experiencing a distinct spectral exchange narrowing through excitonic coupling. In this regard, **ADA1** (**ITIC**) might be considered as a synthetic analog to the chlorophyll aggregates found in natural light harvesting systems (Figure 2b).[32]

Nowadays **ADA1** (**ITIC**) reaches up to 8.7% *PCE* in simple polymer:**ADA1** (**ITIC**) blends with **PBDB-TF**[111] or even up to 10.9% in flexible OSCs exhibiting broadband light trapping.[115] Through chemical modifications of **ADA1** (**ITIC**) and in turn always a change in the resulting solid state packing structure, a further increase in efficiency could be showcased by several derivatives, however all without significant alteration of the spectroscopic signature in comparison to **ADA1** (**ITIC**). Marks and co-workers[111] demonstrated how the end-group fluorination of the DCIND moiety is beneficial for OSC performance. Within a similar slip-stacked J-type packing arrangement with longitudinal slip angles Θ increased from 9/10° to 11/13°, this approach allows sixfold fluorinated derivative **ADA2 (ITIC-6F)** to have lowered π–π distances of down to 3.28 Å and increased electron transfer integrals of up to 56.8 meV, explaining an increase in *PCE* from 8.7% to 11.9% in BHJ OSCs of **ADA2** (**ITIC-6F**) with **PBDB-TF**.

Along another avenue, Li and co-workers investigated a modification of the core substituents by *meta*- instead of *para*-alkyl-phenyl substitution in **ADA3** (***m*-ITIC**).[116] Through improved crystallinity, increased tinctorial strength, and better electron mobility, **ADA3** (***m*-ITIC**) shows an improved *PCE* of about 11.8% as opposed to 10.6% for **ADA1** (**ITIC**) in BHJ OSCs with polymer **J61**. The influence of core-substitution as a main driving force for the slip-stacked packing arrangement was also demonstrated by Li and co-workers through core alkoxy substitution of linear A-D-A dye **ADA4** (**IDIC-2F**).[117] An attachment and subsequent lengthening of alkoxy chains at the donor core led to an increase in 3D network and slip-stacked packing motif formation, effectively increasing the *PCE* in BHJ OSCs with **PBDB-TF**, also known as **PM6**, from 11.5% for unsubstituted **ADA4** (**IDIC-2F**) to 13.0% for decyloxy-substituted derivative **ADA5** (**DO-IDIC-2F**).

A final possibility for modification of **ADA1** (**ITIC**) is the donor core modification as demonstrated by Ding and co-workers for NFA **ADA6** (**CO*i*8DFIC**).[118] With its sterically less shielded core unit, **ADA6** (**CO*i*8DFIC**) can be directed into both face-to-face and slip-stacked packing structures simultaneously through a careful control of spin-casting parameters, allowing for harnessing of both types of aggregates within one active layer. We would like to note that in such cases also contributions from CT interactions could be of importance, as discussed for D-A-D-type squaraine dyes. Through the resulting broadened absorption feature by both hypso- and bathochromically shifted bands and an increase in electron mobility (μ_e) by one order of magnitude, the *PCE* of BHJ OSCs with **PTB7-Th** was increased from 9.3% for lamellar structures to 13.8% for the cooperated both face-to-face and slip-stacked arrangements.[119] In contrast to the following example of **ADA7** (**Y6**), all so far discussed NFAs show only minor bathochromically shifted absorption bands in the solid state which we attribute to a combination of polarization effects, weak J-type Coulomb coupling as well as modest CT-contributions originating from LUMO–LUMO interactions between tightly stacked DCIND moieties.

Another small-molecule A-D-A-type NFA worth highlighting within the context of the impact of molecular packing arrangement on OSC performance is **ADA7** (**Y6**). Initially **ADA7** (**Y6**) was demonstrated in OSC by Zou and co-workers in 2019, reaching 15.7% *PCE* in a BHJ OSC with polymer **PBDB-TF** (**PM6**) as donor material.[120] Ever since, **ADA7** (**Y6**) has received a considerable amount of research interest within the OSC community[121] and has been used to fabricate the highest efficiency small-molecule acceptor-based BHJ OSCs to-date with *PCE* of > 18% with donor polymer **D18**.[57] **ADA7** (**Y6**) hereby consists of a dithienothiophenepyrrolobenzothiadiazole D-A'-D core with fluorinated DCIND terminal acceptor moieties, effectively making it an A-D-A'-D-A-type acceptor in a dipolar cisoid conformation. The core moiety is shielded by (branched) alkyl chains to ensure sufficient solubility and simultaneously prevent aggregation into 1D transport channels through direct face-to-face H-type packing motifs,[120] which would be detrimental for device performance.[97]

In its solid state, **ADA7** (**Y6**) retains a planar and cisoid conformation due to its planar D-A'-D core-unit and the DCIND terminal groups (vide supra), similar to the before mentioned dyes **MC1** and **MC2**, respectively. To-date three different polymorphs of **ADA7** (**Y6**) single crystals have been published, exhibiting either a monoclinic[122] or a triclinic[123,124] crystal lattice. In the following, the structure–property relationship of the dipolar **ADA7** (**Y6**) (μ_g = 2.17 D) is illustrated with the extensive study of its crystal structure conducted by Marks and co-workers.[122] **Figure 9**a shows an excerpt of the 3D "honeycomb" percolation network found for the V-shaped **ADA7** (**Y6**) in the solid state which is formed through the presence of four nearest-neighbor dimers D1–4 with π–π distances of below 3.37 Å. This packing structure appears to be again influenced by the antiparallel alignment of the respective partial dipole moments of the acceptor-DCIND units, thereby resembling the packing motif found for many D-A merocyanine dyes.[4,100,101] A similar 3D grid-like packing structure with a comparable multitude of dimers is also found within the triclinic polymorph crystal systems of **ADA7** (**Y6**).[123,124] Within this supramolecular arrangement, both D1 and D2 exhibit an arrangement allowing for an excitonic Coulomb J-type coupling with a Θ of 6° and 9°, respectively, and a resulting $J_{Coulomb}$ as calculated by a point-dipole approximation of –150 to –400 cm^{-1} (19–50 meV). However, D1 shows additional π–π interaction through end-group stacking of the DCIND acceptor units, while D2 shows the possibility for additional CT-mediated coupling through a mismatched stacking of DCIND acceptor and thienothiophene

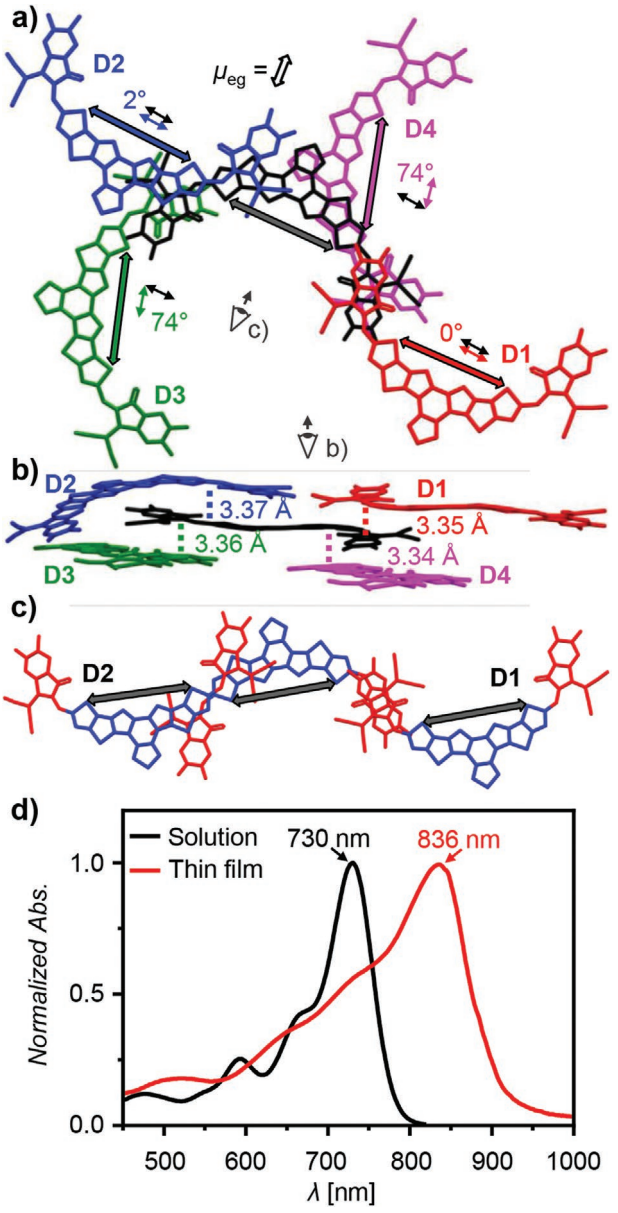

Figure 9. a) Top and b) side view including respective π–π distances of the packing arrangement in the **ADA7** (**Y6**) single-crystal structure according to ref. [122]. The two-headed arrows mark the respective transition dipole moment (μ_{eg}) axis of each molecule. The angular values in a) indicate the rotational angle α between μ_{eg} of the nearest neighbors forming dimers D1 (red), D2 (blue), D3 (green), and D4 (magenta) in respect to the central μ_{eg} (black). c) Top view of dimers D1 and D2, which show a geometrical arrangement suitable for a conventional J-aggregation according to Kasha, with the acceptor and donor units highlighted in red and blue, respectively. Alkyl chains and hydrogen atoms have been omitted for clarity. d) Solution (black) and thin film (red) absorption spectra of **ADA7** (**Y6**).

donor moieties. Dimers D3 and D4 meanwhile should barely contribute to excitonic coupling due to a large rotational angle (α) of 74° between their μ_{eg} of 10.7 D in respect to that of the central chromophore. D3 hereby shows end-group stacking of the rigid DCIND unit, while D4 is the only dimer showing significant π-overlap of the chromophore core due to the alkyl substituents preventing additional tight face-to-face packing arrangements of the other dimers. This myriad of interactions in turn leads in contrast to the **ADA1** (**ITIC**) derivatives to a significant bathochromic shift of about 106 nm (1740 cm^{-1}) up to 836 nm along with a spectral broadening of the absorption spectrum of **ADA7** (**Y6**) in the solid state (Figure 9b). Accordingly, the structural and optical features of **ADA7** (**Y6**) seem to favorably relate to high *PCE* values through a resulting higher J_{sc} by multidimensional percolation pathways within the porous 3D "honeycomb" network.

Analogous to the previously described D-A-D dyes (Section 3.1), in A-D-A-type NFAs, the decrease of the $S_0 \rightarrow S_1$ transition energy due to intermolecular coupling contributes to the harvesting of NIR light, thereby improving the J_{sc} and *PCE*.[119,125] Interestingly, most NFA-based OSCs show efficient charge separation and low voltage loss characteristics despite a small energetic offset between the intermolecular CT state and the lowest local excited state, which in general is the S_1 state of an NFA. Numerous studies have been conducted on the nature of interfacial CT states and energy loss in recent years, but the precise origins of low energy loss are still unclear.[15,16,126] While the latest results related to energy loss have been well summarized by Nguyen and co-workers.[15] We would like to especially denote the following points: 1) Within NFA materials, the slip stacking can induce a reduced S_1 state energy and the small energy offset.[127] 2) Along with this low energy offset, excellent electronic coupling leads to the hybridization of the donor-acceptor-interfacial singlet CT states (^{1}CT) with the relatively high-emissive J-coupled NFA S_1 states.[128] 3) These hybridized S_1-CT states seem to play an important role in small voltage loss.[129–131]

In summary, the formation of slip-stacked packing arrangements with J-type Coulomb coupling augmented by CT-mediated J-coupling based on donor–acceptor interaction proved to be beneficial for both D-A-D squaraine donor as well as A-D-A dye NFAs utilized in BHJ OSCs. The interplay and balance of structure-directing intermolecular forces such as π–π and (partial-)dipole–dipole as well as function-directing Coulomb and CT coupling interactions play a key role in the molecular design, which are as important as the molecule's opto-electronic properties. For a comprehensive interpretation, the definition of a J-aggregate hereby needs to be broadened with respect to the classical definition given by Kasha, as J-type aggregates observed in thin films of D-A-D squaraine dye donor materials or A-D-A NFAs exhibit a multitude of predominant intermolecular interactions in addition to $J_{Coulomb}$ according to the simple Kasha picture. This myriad of long-range (Coulomb) and short-range (orbital) interactions in slip-stacked packing structures leads to bathochromically shifted but spectrally broadened absorption spectra, enabling panchromatic absorption up to the NIR which significantly contributes to the extracted photocurrent, while retaining the geometric benefits such as an extended π-overlap within the slip-stacked structure for efficient exciton and charge transport. The latter point for sure plays a major role for the recent impressive improvements for solution-processed OSCs compared to vacuum-processed ones. Due to the required sublimation, the latter are limited to rather small molecular scaffolds that cannot be tailored for such sophisticated packing arrangements as illustrated in Figure 9 for **ADA7** (**Y6**).

4. Organic Photodetectors

In addition to the application in OSCs as discussed in Section 3, organic semiconductors are also promising materials for photodetectors.[132–136] Owing to the stable performance and the mature fabrication technology, most of today's state-of-the-art commercial photodetectors are based on crystalline silicon (Si) or indium gallium arsenide (InGaAs). However, inherent weak and broadband absorption characteristics of inorganic semiconductors require thick active layers and additional color filter systems for wavelength resolved imaging sensors (**Figure 10**a). These drawbacks of inorganic semiconductors inherently limit their applicability in flexible devices and future applications. Organic semiconductors have been investigated as alternative photosensitizing materials for imaging sensors due to their mechanically soft and optically tunable properties,[133] and based on the efficient photocurrent generation of these materials in a BHJ device structure, OPDs have shown high performances matching or even exceeding those of inorganic photodetectors.[137–139] In addition, recently developed NFAs can further improve the photogeneration efficiency and extend the spectral photoresponse range from visible to NIR light in BHJ OPDs.[140,141]

As shown in Figure 10b, the stacking of multiple narrowband photodetectors is ideal for developing compact device structures capable of multispectral or hyperspectral image sensing, which are highly desirable for emerging applications such as biomedical imaging, environmental monitoring, and machine vision.[132] However, most organic semiconductors applied so far in BHJ OPDs originated from research on broadband-absorbing OSCs and as such exhibit panchromatic absorption properties. In order to develop narrowband OPDs based on a panchromatic absorbing BHJ thin film, several elegant device design strategies have been demonstrated in recent years such as charge collecting narrowing (CCN)[142,143] and microcavity-induced narrowing,[144] exhibiting spectral response widths below 100 nm. However, these approaches require precisely controlled and rather thick active layers (> 1 µm) or a fully as well as a partially reflective electrode, which inhibits the possibility of implementing such sensors in efficient stacked imaging architectures as displayed in Figure 10.

In contrast to these device-engineering-based approaches, the development of inherently narrowband absorbing photoactive materials, either intrinsic or due to J-type coupling, constitutes the most straightforward strategy for developing future stacked imaging sensors by molecular design without the need of additional device engineering.[135,145] In order to design narrowband absorbing molecules, the structural relaxation process upon photoexcitation should be minimized. Thus, the best starting point are dyes that already exhibit intense and narrow monomeric absorption spectra with little coupling to vibrational modes as found for cyanine or squaraine dyes due to their similar ground and excited state geometries (i.e., little bond length alternation and small reorganization energy upon excitation).[146,147] Furthermore, these dyes should either experience negligible interactions with neighboring dyes in the solid state to retain their monomeric absorption features or, even better, experience band narrowing as demonstrated in Figure 2a in Section 2 for strongly J-coupled cyanine dyes. This unique property of J-aggregates of cyanine dyes inspired the development of narrowband digital photodetectors analogous to their application as photosensitizers in color film photography.[19,20] In the following sections, we will provide a short overview on the most important OPD performance parameters followed by a presentation of recent achievements in narrowband OPDs based on ionic cyanine as well as neutral ketocyanine, merocyanine, and squaraine dyes. By comparing the spectral response width of monomeric and aggregated chromophores in their respective solid state along with representative examples of the molecular packing, we will demonstrate the advantage of strongly exciton coupled dye aggregates for developing future ultra-narrowband OPDs.

4.1. Performance Parameters of Organic Photodetectors

In contrast to OSCs, which aim toward achieving a high *PCE* for harvesting of terrestrial sun light, it is hard to define a single parameter to quantify overall OPD performance due to the key parameters depending strongly on the desired application. Therefore, before introducing the recent progress in narrowband OPDs, we will briefly explain the most relevant

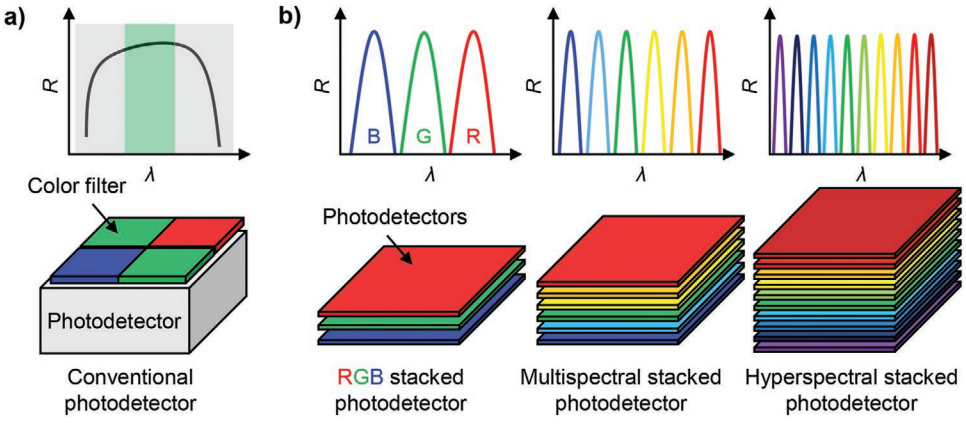

Figure 10. Schematic responsivity (*R*) spectra (top) and imaging sensor structures (bottom) of a) conventional panchromatic photodetectors with color filters and b) stacked (ultra)narrowband photodiodes envisioned for future applications (R: red, G: green, B: blue).

figures of merit required for describing the efficiency, spectral selectivity, and operating speed limit of OPDs. The photoconversion efficiency of OPDs can be described by either the external quantum efficiency (*EQE*) or responsivity (*R*). *EQE* is the ratio between the number of photogenerated carriers (n_e) per incident photons (n_{ph}) as a function of the wavelength

$$EQE = \frac{n_e}{n_{ph}} \tag{2}$$

R is defined as the generated photocurrent (I_{ph}) per incident optical power (P_{light}) as a function of the wavelength

$$R = \frac{I_{ph}}{P_{light}} = EQE \times \frac{q\lambda_{input}}{hc} \tag{3}$$

where q is the elementary charge, λ_{input} is the wavelength of incident light, h is the Planck constant, and c is the speed of light. In contrast to OSCs, OPDs can be operated both under reverse bias ($V < 0$ V) and short-circuit conditions ($V = 0$ V), depending on the respective application.[148] An external reverse bias usually increases the *EQE* and *R* because of enhanced exciton dissociation and charge extraction. However, high reverse bias typically also coincides with increased dark current levels of the OPD, impairing the signal-to-noise ratio. To evaluate the signal-to-noise ratio, the specific detectivity (*D**) should be considered as the most important parameter for general OPDs. This figure of merit describes the achievable signal-to-noise ratio normalized to an active area of 1 cm^2 with an electrical bandwidth of 1 Hz at an incident input light power of 1 W as

$$D^* = \frac{R\sqrt{A\,\Delta f}}{i_{noise}} \tag{4}$$

where A is the area of the active layer, Δf is the electrical bandwidth, and i_{noise} is the noise current consisting of the shot noise (i_{shot}), thermal noise ($i_{thermal}$), and flicker noise ($i_{flicker}$) components.[149] Because i_{shot} is linearly proportional to the dark current, i_{shot} is the dominant component of i_{noise} under high reverse bias conditions and as such can be estimated at these conditions (shot-noise limit approximation).

In order to quantify the spectral selectivity of OPDs, the wavelength at the maximum *EQE* ($\lambda_{max,EQE}$) and the corresponding full-width at half-maximum ($FWHM_{EQE}$) are commonly reported. It should be emphasized that these parameters are equally important to *D** for narrow-band OPDs. Further, for determining the operation speed of OPDs, the cut-off frequency (f_{-3dB}) is an important parameter, which is defined as the modulation frequency at which the responsivity of OPDs is reduced to −3 dB (≈70.8% of the photocurrent amplitude at steady-state conditions). More detailed explanations on OPD parameters and measurement setups can be found in the literature.[134]

4.2. Cyanine and Ketocyanine Dye Aggregates

Cyanine dyes are cationic polymethine chromophores where electron-donating aromatic heterocyclic groups are connected through an odd number of sp^2-hybridized carbons.[22] In the ideal polymethine state,[150] π-electrons are perfectly delocalized along the entire π-conjugated system and the polymethine chain adopts nonalternating bond lengths in the electronic ground state (S_0).[22,146] This ground state geometry is similar to that of the first excited state (S_1, HOMO → LUMO transition), leading to an only minimal geometry change upon electronic excitation ($S_0 \rightarrow S_1$) and small vibronic progression.[147] Therefore, cyanine dyes show characteristic sharp and intense absorption spectra as monomers in solution. As discussed in Section 2, the absorption spectra of their strongly excitonic coupled J-aggregates originate mainly from Coulomb coupling and show bathochromically shifted and further exchange narrowed absorption bands with a reduced vibronic progression compared to their monomers (Figure 2).[53] This unique optical property has promoted the development of photodetectors using cyanine dyes and J-aggregates thereof which are summarized in **Figure 11** and their respective characteristic OPD properties collected in **Table 3**. It is noteworthy that the photoconductivity of cyanine dyes has indeed already been reported by Nelson in the 1950s,[151] but that the covered wavelength range of the available OPDs for cyanine dyes in Table 3 does not include blue light-selective OPDs.

Although several OPDs based on amorphous or weakly aggregating cyanine dyes showed wavelength-selective photodetection characteristics with $FWHM_{EQE}$ of down to about 100 nm, most still exhibit a broad spectral response in the final device (**Cy7**–**10**). Hany and co-workers demonstrated in 2015 NIR detecting transparent OPDs based on **Cy7** using a PHJ structure with photo-polymerized C_{60} as acceptor layer, which exhibited an appreciably high *EQE* of 23% and an $FWHM_{EQE}$ of about 130 nm at $\lambda_{max,EQE} = 850$ nm under −2 V conditions.[152] Here, the broad spectral absorption occurs due to the amorphous nature of the spin-coated **Cy7** thin film which lacked the desired band narrowing.[153] Lunt and co-workers investigated OSC and OPD properties of **Cy8**-based devices depending on various counter ions. Despite sharp absorption spectra in solution, spin-coated thin films exhibited broadened *EQE* spectra in the respective devices ($FWHM_{EQE}$ ≈200 nm, $\lambda_{max,EQE} = 880$ nm).[154] In their following research, NIR-sensitive OPDs based on **Cy9** and **Cy10** with even broader spectral responses were reported ($FWHM_{EQE} >> 200$ nm).[155]

Like ionic cyanine dyes, neutral ketocyanine dyes also exhibit narrow absorption spectra in their monomeric state. The fact that the absorption selectivity of **Cy11**–**13** is located at rather low wavelengths (510–525 nm) suggests that the delocalization does not extend along the whole polymethine chain like for the other dyes shown in Figure 11. This enables, however, an extension of the spectral range for cyanine dye-based OPDs toward green light selectivity. Burn and co-workers developed ketocyanine-based OPDs, including **Cy11** and **Cy12**, as light absorbing materials in narrow-band photodetectors,[156] showing green light selectivity ($FWHM_{EQE} < 175$ nm) with OPDs of **Cy12** exhibiting an EQE_{max} of 8.2% and $FWHM_{EQE}$ of 130 nm at $\lambda_{max,EQE} = 510$ nm. Meredith and co-workers reported further optimized green selective OPDs by combining narrow absorbing ketocyanine dyes (**Cy11** and **Cy13**) and optical cavity tailoring.[157] Their optimized OPD containing **Cy13** exhibited a narrow spectral response ($FWHM_{EQE} = 80$ nm) with an *EQE* of 15% at $\lambda_{max,EQE} = 525$ nm.

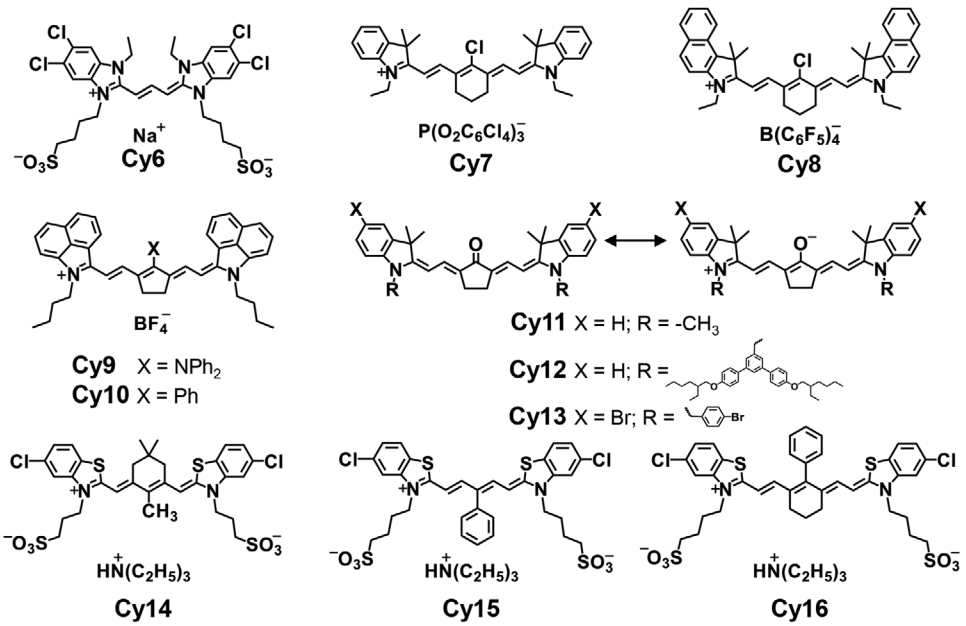

Figure 11. Molecular structures of anionic (**Cy6** and **Cy14-16**) and cationic cyanine dyes (**Cy7-10**) and neutral ketocyanines (**Cy11-13**).

Compared to the so far discussed devices based on amorphous or weakly aggregating chromophores, OPDs of J-aggregates of cyanine dyes exhibit a significantly more selective photospectral response due to their exchange narrowed optical absorption spectra.[158–161] Unfortunately, the molecular arrangement or even the single-crystal structures of the employed J-aggregates of the following cyanine dyes (**Cy6** and **Cy14–16**) are not reported in literature, making it difficult to establish a clear structure–property relationship. However, considering the ratio of the intensities of the respective 0–0 and 0–1 bands in their aggregated states, these dyes presumably have a strong J_{Coulomb} (**Figure 12**a,b). Bulović and co-workers reported high *EQE* values of up to 16.1% ($\lambda_{\text{max,EQE}}$ = 756 nm) based on J-aggregating **Cy14** single-layer OPDs with ZnO and MoO_3 as electron and hole transport layers, respectively (Figure 12a).[162] However, the corresponding *EQE* spectrum remained broadened ($FWHM_{\text{EQE}} \approx 130$ nm) relative to the thin-film spectrum of **Cy14** ($FWHM \approx 30$ nm) due to interference effects from the

Table 3. Summary of the optical and device properties of OPDs based on cyanine dyes.

Materials[c)]	Optical[a)]		Device[b)]							Ref.
	λ_{max} [nm]	*FWHM* [nm]	$\lambda_{\text{max,EQE}}$ [nm]	$FWHM_{\text{EQE}}$ [nm]	*EQE*(@V_{bias}) [%]	*R* [mA W^{-1}]	D^*_{max} [10^{11} Jones]	$f_{-3\text{dB}}$ [kHz]	Active layer(s)	
[**Cy6**]$^-$[Na]$^+$	586	10[d)]	586	28	6 (@ 0 V)	28	0.003	3.6	PHJ	[163]
[**Cy7**]$^+$ [TRISPHAT]$^-$	830[d)]	130[d)]	850	130[d)]	23 (@ −2 V)	165	10	–	PHJ	[152]
[**Cy8**]$^+$[TPFB]$^-$	850[d)]	200[d)]	880	200[d)]	21 (@ 0 V)	150[e)]	–	–	PHJ	[154]
[**Cy9**]$^+$[BF_4]$^-$	1200[d)]	450[d)]	1200	500[d)]	2.1 (@ 0 V)	20[e)]	0.04	–	PHJ	[155]
[**Cy10**]$^+$[BF_4]$^-$	1400[d)]	400[d)]	1350	600[d)]	1.4 (@ 0 V)	15[e)]	0.07	–	PHJ	[155]
Cy11	527	117	520	175	8.0 (@−1 V)	34[e)]	–	–	BHJ	[156]
Cy11	527	117	525	90	17 (@−1 V)	72[e)]	–	20	BHJ	[157]
Cy12	522	101	510	130	8.2 (@−1 V)	34[e)]	0.03[f)]	–	BHJ	[156]
Cy13	524	108	525	80	15 (@−1 V)	64[e)]	–	25	BHJ	[157]
[**Cy14**]$^-$[TEA]$^+$	790	30[d)]	756	130[d)]	16.1 (@ 0 V)	98[e)]	4.3	92	SL	[162]
[**Cy15**]$^-$[TEA]$^+$	780	50[d)]	780	72	14 (@ 0 V)	88	0.1	3.5	PHJ	[163]
[**Cy16**]$^-$[TEA]$^+$	980	30[d)]	980	50	3.1 (@ 0 V)	25	0.01	20	PHJ	[163]

[a)]The wavelength absorption maximum (λ_{max}) and its full-width at half-maximum (*FWHM*) in the neat thin film; [b)]The *EQE* maximum wavelength ($\lambda_{\text{max,EQE}}$) and its full-width at half-maximum ($FWHM_{\text{EQE}}$) in the thin film device. Active layer: single-layer (SL); [c)]Counterions: *tris*(tetrachloro-1,2-benzenediolato)-phosphate(V) (TRISPHAT$^-$), tetrafluoroborate (BF_4^-), tetrakis(pentafluorophenyl)borate (TPFB$^-$), triethylammonium (TEA$^+$); [d)]Values were estimated from the graphical data provided in the literature; [e)]Values were estimated according to Equation (3); [f)]Values were estimated according to Equation (4) as well as the shot noise limit estimation.

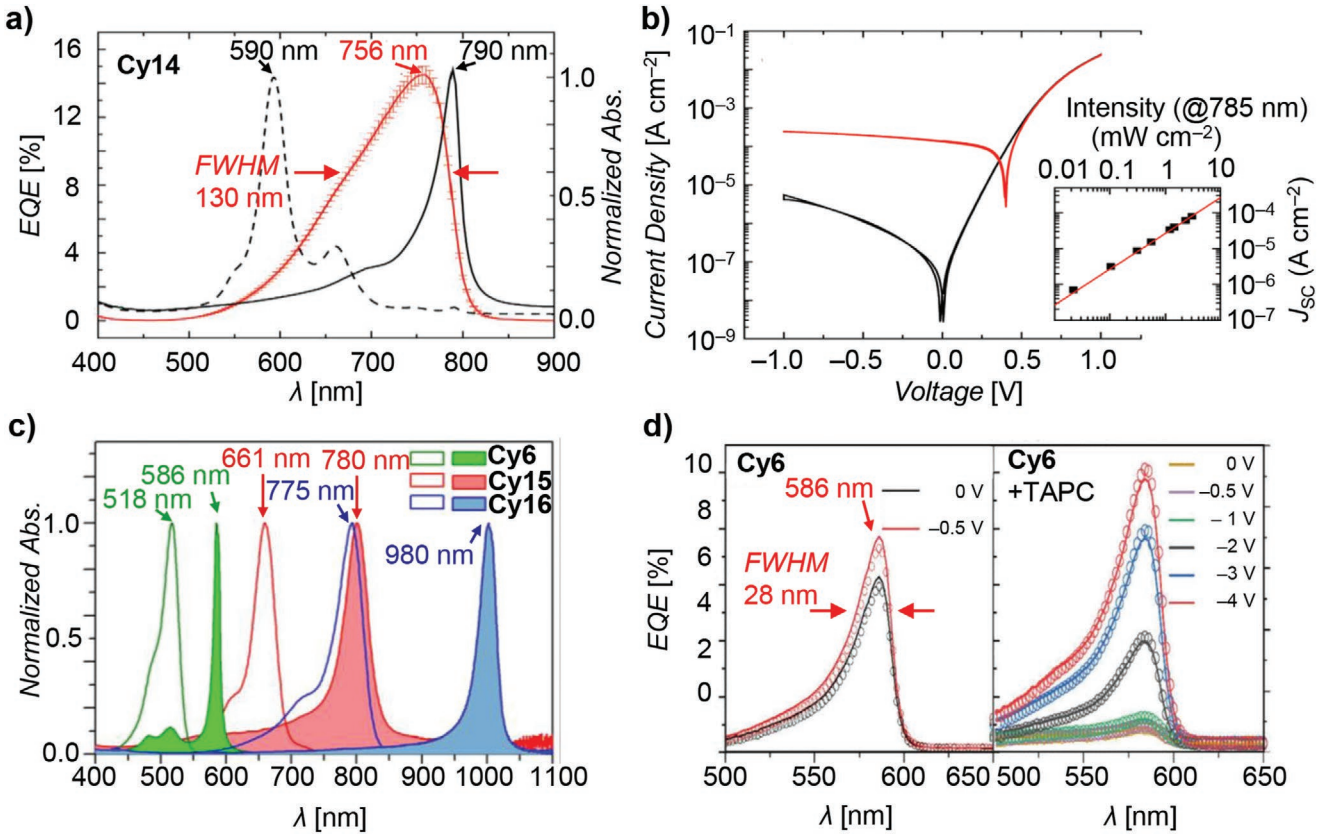

Figure 12. a) Absorption spectra of **Cy14** in solution (black dashed) and J-aggregate thin films (black solid), and the *EQE* spectrum (red solid) of its OPD. b) Current–voltage characteristics in dark (black solid) and under illumination (red solid) corresponding to **Cy14**-based OPD. a,b) Adapted with permission.[162] Copyright 2012, American Institute of Physics. c) Absorption spectra of **Cy6**, **Cy15**, and **Cy16** in monomer (open, in methanol) and J-aggregate states (filled, in aqueous solution). d) *EQE* spectra of [**Cy6**]$^-$[Na]$^+$ OPDs without (left) and with electron blocking layer (right). c,d) Adapted with permission.[163] Copyright 2019, The Royal Society of Chemistry.

cavity. Moreover, this OPD shows undesired high dark current values under a reverse bias condition, presumably due to the thin and rough active layer (Figure 12b). More recently, Nüesch and co-workers successfully developed efficient narrow-band OPDs based on J-aggregates of **Cy6**, **Cy15**, and **Cy16** that covered an impressive wavelength range from 586 nm up to 980 nm (Figure 12c).[163] In order to prepare high-quality J-aggregate thin films, they optimized the thin-film deposition conditions (**Cy6**: spin-coating the aqueous J-aggregate solution; **Cy15** and **Cy16**: spin-coating the monomer solution). The optimized **Cy6**, **Cy15**, and **Cy16** OPDs exhibited $EQE/FWHM_{EQE}$ values of 6%/28 nm ($\lambda_{max,EQE}$ = 586 nm), 14%/88 nm ($\lambda_{max,EQE}$ = 780 nm), and 3.1%/25 nm ($\lambda_{max,EQE}$ = 980 nm), respectively. To minimize the detrimental dark current due to pinholes in the rough and thin layer of the **Cy6** J-aggregate, they introduced an additional 50 nm thick vacuum-deposited 4,4′-cyclohexylidenebis[*N*,*N*-bis(4-methylphenyl)benzenamine] (TAPC) electron blocking layer. Although the thick blocking layer could effectively reduce the dark current, unfortunately the photocurrent and *EQE* decreased as well (Figure 12d).

Although J-aggregating ionic cyanine dyes afford interesting narrow spectral responses in OPDs, improving device performance remains challenging. As commented on in Nüesch et al.'s work, high-quality J-aggregate thin films with a smooth surface and low density of pinholes and grain boundaries are difficult to prepare.[163] Because most cyanine dyes have a lamellar-like packing structure with edge-on orientation on a substrate, they can only provide a short exciton diffusion length (L_D = 2.0 ± 0.4 nm) along the thin-film surface normal,[162] which is the most significant direction for transport in OPDs to reach neighboring interfaces. Thus, the thickness of most cyanine dye thin films in the optimized single layer or PHJ OPDs is very thin (typically around 10 nm), which can limit efficient photocurrent generation and increases device's dark current levels. Similar to high-performing OSCs, fabricating BHJ OPDs is one possible solution for this problem. However, due to the commonly ionic character of cyanine dyes, it is hard to fabricate BHJ devices with conventional neutral acceptors.[164,165] Low miscibility with such acceptor molecules can cause significant phase separation and a resulting rough morphology, which is detrimental for the performance of BHJ devices. Furthermore, the optoelectronic properties are dependent on the respective counterion[154,155] and mobile counter ions are known to induce a space charge under external bias conditions,[166] limiting cyanine dye-based OPDs operating under reverse bias conditions. Therefore, in addition to ketocyanines, neutral chromophores-like merocyanine and squaraine dyes are promising alternatives, which will be discussed in the subsequent sections.

4.3. Merocyanine Dye Aggregates

Merocyanine dyes are neutral dipolar chromophores which are composed of donor–acceptor (D-A) units connected via a polymethine bridge.[167] Depending on the donor and acceptor strength and length of the polymethine chain, merocyanines can exhibit distinctive spectral and electrooptic characteristics. For the special situation called the cyanine-limit (the resonance parameter $c^2 = 0.5$), whereby a neutral ($c^2 = 0$) and a zwitterionic ($c^2 = 1$) resonance structure contribute equally to the charge distribution (see resonance structures of **MC3** in **Figure 13**), the π-electrons are analogously to cyanine dyes perfectly delocalized over the entire polymethine bridge with almost equal bond lengths, resulting in a narrow and intense absorption band.[168,169] Such a situation can be realized most efficiently by including quinoidal heterocyclic subunits within a polymethine chain between strongly electron-donating (e.g., dimethylamino) and electron-withdrawing (e.g., nitro, dicyanomethylene) groups.[170] Along with desired optical properties, merocyanine dyes in the cyanine-limit inherit a minimized reorganization energy both for optical excitation and hole or electron transfer, which is also beneficial for OSCs as well as color selective photodetectors.[171] Already in 1981, Kudo and Moriizumi demonstrated the first OPD based on merocyanine dye PHJ devices.[172] Even in this pioneering work, they mentioned the potential feasibility of organic dyes for color-filter-free photodetectors. Indeed, the utilized merocyanine-based OPDs already exhibited green color-selective photocurrent with a *FWHM* value of about 110 nm. However, in the following years, merocyanines received little attention as organic semiconductors because their high dipolarity was considered unfavorable for charge carrier transport. Nevertheless, a large variety of these dipolar dyes were synthesized for applications in nonlinear optics and photorefractive materials.[173,174] Among the series of chromophores, several dyes could be identified at the cyanine-limit and in the subsequent years clear structure–property relationships could be established that enabled the optimization of the molecular properties for the envisioned applications such as electro-optical modulation and photorefractive effects.[175] Later on this knowledge was extended for the design of organic semiconductors for OTFTs[176] and as efficient donor materials in OSCs.[101,177,178] More recently, like for cyanine dyes, excitonically coupled aggregates and solid-state materials with reduced *FWHM* of their absorption bands could be designed through the interplay of strong dipole–dipole interactions along with sterical shielding or substituent-directed supramolecular organization.[7,179] The most relevant molecular structures of employed merocyanine dyes in OPDs are depicted in Figure 13 and their respective device properties are listed in **Table 4**.

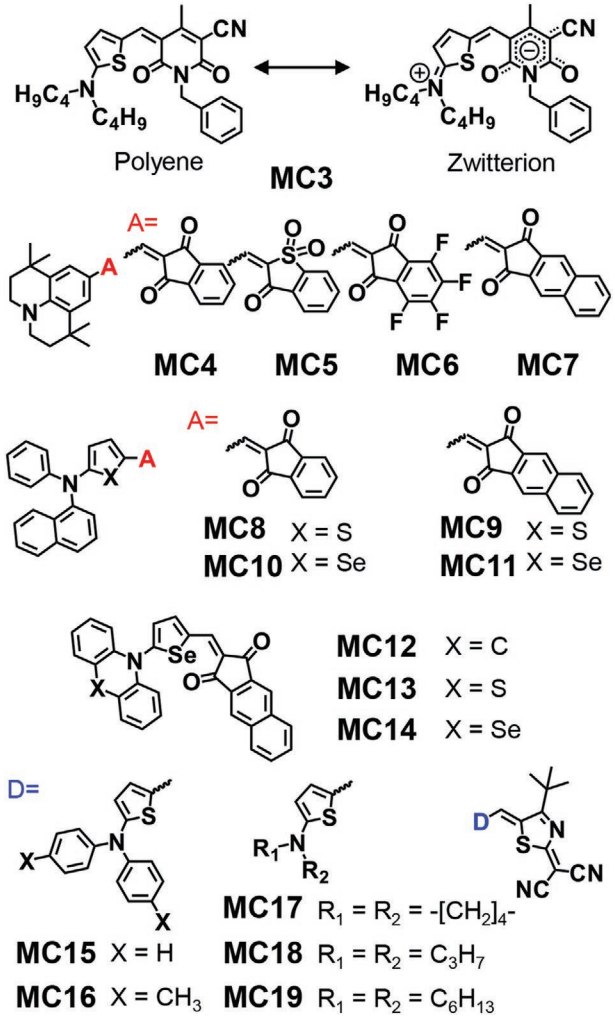

Figure 13. Molecular structures of merocyanine dyes.

Efficient narrow-band but mainly green-selective BHJ OPDs in combination with fullerene derivatives have been reported based on amorphous or weakly aggregating dyes (**MC3–14**), typically exhibiting $FWHM_{EQE}$ values of around 100 nm. Here, in the context of their research on merocyanine-based PHJ and BHJ OSC devices (vide supra).[99–101,103,180,181] Meerholz and coworkers noted that some of these BHJ devices indeed showed an excellent green color-selective photoresponse while their OSC performance was rather modest, e.g., **MC3** with $EQE = 42\%$, $FWHM_{EQE} \approx 100$ nm, $\lambda_{max,EQE} \approx 550$ nm, and $PCE = 1.22\%$ for the OSC.[103] Following this work, the Samsung Electronics Company has reported a series of green-selective OPDs based on merocyanine dyes over the last years.[182–185] In 2016, **MC4–7** were reported bearing a julolidine and 1,3-indandione moiety as the electron-donating and -accepting groups, respectively[182] While all of these dyes showed a green light-selective photoresponse, the optimized vacuum-deposited **MC7**:C_{60} BHJ OPD stood out, exhibiting an *EQE* of 48.6% and an $FWHM_{EQE}$ of 97 nm at $\lambda_{max,EQE} = 550$ nm. In following works, **MC8–11** were reported bearing popular amino-thiophene[170] and amino-selenophene units as donor moieties to tune the push–pull dyes' characteristics toward the cyanine-limit.[183,184] The optimized vacuum-deposited **MC10**:C_{60} BHJ OPD showed an *EQE* of 51.8% and an $FWHM_{EQE}$ of 97 nm at $\lambda_{max,EQE} = 560$ nm. Subsequently, **MC12** to **MC14** were reported with different donor moieties.[185] The vacuum-deposited **MC14**:C_{60} BHJ OPD exhibited a higher *EQE* value of up to 65.9% at 550 nm but a slightly broadened $FWHM_{EQE}$ value of 125 nm. Accordingly, these OPDs show their limitation in the photoresponse bandwidth, which is a consequence of the bulky substituents at the donor moieties that prohibit these merocyanine dye from

Table 4. Optical and device properties of OPDs based on merocyanine dyes.

Materials	Optical[a]		Device[b]							Ref.
	λ_{max} [nm]	*FWHM* [nm]	$\lambda_{max,EQE}$ [nm]	$FWHM_{EQE}$ [nm]	*EQE* (@ V_{bias}) [%]	*R* [mA W^{-1}]	D^*_{max} [10^{11} Jones]	f_{-3dB} [kHz]	Active layer(s)	
MC3	558	100[c]	550[c]	110[c]	42 (@ 0 V)[c]	190[d]	-	-	BHJ[f]	[103]
MC4	525	90	520	90[c]	42.4 (@ −3 V)	178[d]	7[e]	–	BHJ	[182]
MC5	526	98	520	100[c]	44.3 (@ −3 V)	186[d]	2[e]	–	BHJ	[182]
MC6	548	97	530	100[c]	38.8 (@ −3 V)	166[d]	10[e]	–	BHJ	[182]
MC7	552	100	550	97	48.6 (@ −3 V)	216[d]	400[e]	–	BHJ	[182]
MC8	515	83	530	98	47.5 (@ −3 V)	203[d]	70[e]	–	BHJ	[183]
MC9	547	83	550	101	52.0 (@ −3 V)	231[d]	120	–	BHJ	[183]
MC10	560	80	560	97	51.8 (@ −3 V)	234	40	–	BHJ	[184]
MC11	534	79	540	102	46.7 (@ −3 V)	203	10	–	BHJ	[184]
MC12	–	–	565	128	51.1 (@ −3 V)	233	–	–	BHJ	[185]
MC13	567	93	555	125	54.1 (@ −3 V)	242	–	–	BHJ	[185]
MC14	564	91	550	125	65.9 (@ −3 V)	292	800	10	BHJ	[185]
MC15	742	30	747	30	9 (@ 0 V)	55	0.9	–	PHJ	[187]
MC16	749	36	750	65	5 (@ 0 V)	31	0.3	–	PHJ	[187]
MC17	479	17	481	76	18 (@ 0 V)	71	2	–	PHJ	[187]
MC17	477	17	480	27	15 (@ 0 V)	58	0.3	180	PHJ	[188]
MC18	746	24	–	–	–	–	–	–	PHJ	[187]
MC19	750	19	750	11	14 (@ 0 V)	85	0.2	150	PHJ	[188]

[a]The wavelength absorption maximum (λ_{max}) and its *FWHM* in the neat thin film; [b]The *EQE* maximum wavelength ($\lambda_{max,EQE}$) and its full-width at half-maximum ($FWHM_{EQE}$) in the thin film device; [c]Values were estimated from the graphical data provided in the literature; [d]Values were estimated according to Equation (3); [e]Values were estimated according to Equation (4) as well as the shot noise limit estimation. f) OSC.

closely stacked packing and therefore strong exciton coupling (vide supra).

To further reduce the spectral bandwidth of OPDs, our group has aimed at controlling the molecular packing arrangement and excitonic coupling of highly dipolar merocyanine dyes close to the cyanine limit in the solid state by means of properly positioned substituents (**Figure 14**a). Due to their large ground state dipole moments, merocyanine dyes in the cyanine limit have a high propensity for the formation of antiparallelly aligned face-to-face stacking arrangements that exhibit rather H- than J-type excitonic coupling (Section 3.2). However, in thin films, i.e., in the solid state, by modulating the size of the aliphatic or aromatic substituents at the amine donor substituent and with support of the sterically demanding *tert*-butyl group at the acceptor heterocycle, cofacial stacking becomes unfavorable and instead slip-stacked zig-zag arrangements are induced (Figure 14b,c).[179] This unique zig-zag packing of head-to-tail aligned dipolar dyes does not only yield ultra-narrow absorption bands ($FWHM$ = 16 nm (280 cm^{-1})) of strongly Coulomb coupled J-aggregates, but also provides an efficient 2D network with charge carrier mobilities as high as 0.64 cm^2 V^{-1} s^{-1} in the neat crystalline thin film.[186] Based on these results, thin films of strongly excitonic coupling merocyanine dyes with selective absorption of either blue (e.g., **MC17**; H-type $J_{Coulomb}$) or NIR (e.g., **MC15**, **MC16**, **MC18**, and **MC19**; J-type $J_{Coulomb}$) light and *FWHM* values of less than 50 nm in their respective thin films could be prepared (Figure 14d) and applied in ultra-narrow band OPDs in PHJ architectures with C_{60}.[187] **MC15**-based devices hereby exhibited an *EQE* of 9% and an $FWHM_{EQE}$ of 30 nm at $\lambda_{max,EQE}$ = 747 nm. Subsequently, dual-band absorbing OPDs with mixed social-self-sorting **MC17**:**MC19** thin films (Figure 14e)[188] were fabricated which afforded an extremely narrow-band photoresponse in the NIR region at $\lambda_{max,EQE}$ = 750 nm with an *EQE* as high as 14% and $FWHM_{EQE}$ of only 11 nm in an optimized PHJ OPD with C_{60}.

4.4. Squaraine Dye Aggregates

Squaraine dyes as neutral D-A-D chromophores exhibit cyanine-like intense and narrow absorption bands with only weak vibronic progressions, which can be further shifted to the NIR by dicyanomethylene acceptor-substitution of the central squaric acid unit (**Figure 15**a,b).[79,189] Similar to merocyanine dyes in the cyanine limit, their electronic structure can be explained by a mesomerism involving contributions of one neutral and two degenerate zwitterionic states with the nitrogen-containing aromatic units as donor moieties and the central squaric acid as an acceptor moiety.[50] However, while strong dipole–dipole interactions between the D-A scaffold of merocyanine dyes strongly favor the antiparallel cofacially stacked aggregate both in solution and the solid state, the aggregation behavior of squaraine dyes is more flexible and governed by a combination of dispersion, electrostatic, and CT interactions between the chromophores. In solution, mostly cofacial stacking guided by dispersion and dipole–dipole interactions

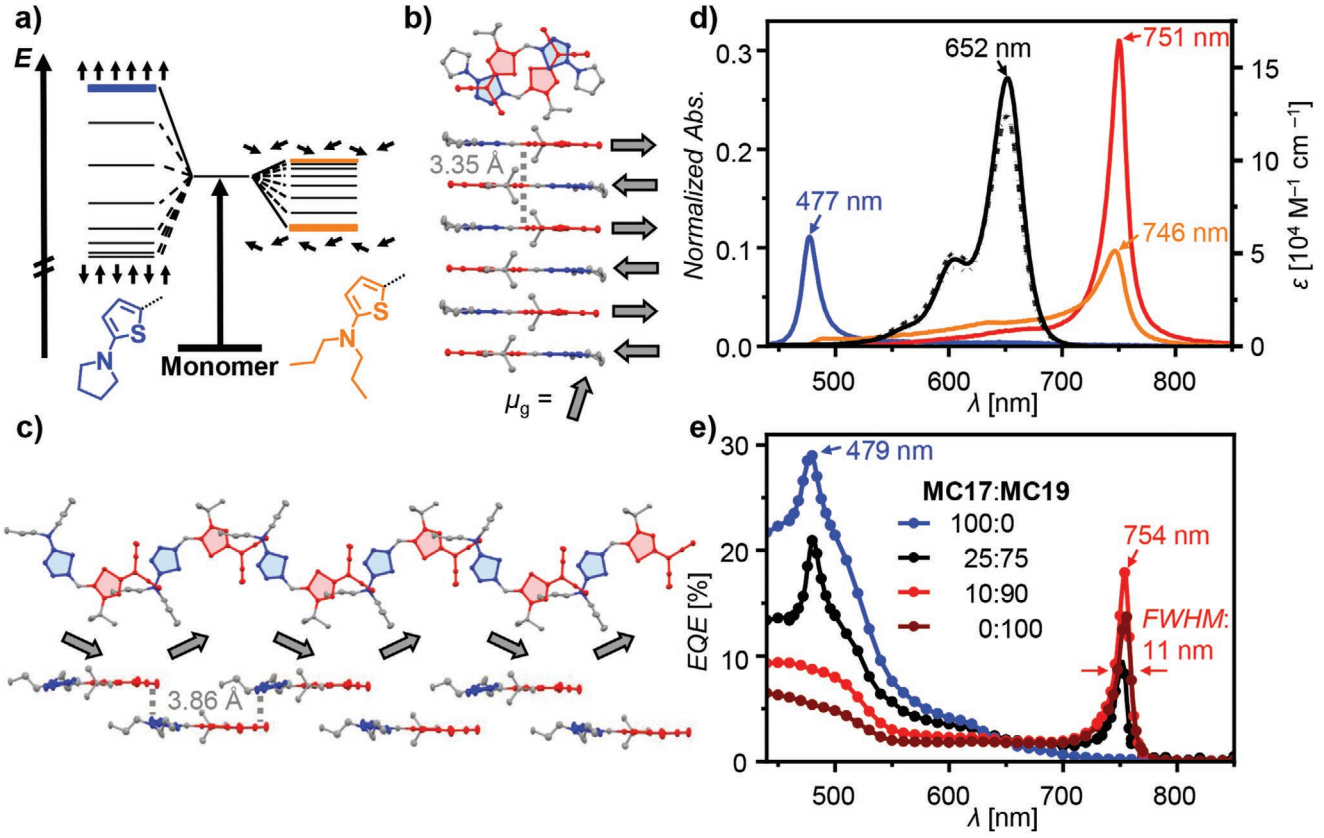

Figure 14. a) Schematic illustration of the exciton band diagram of **MC17** and **MC18**. Molecular packing structures of b) **MC17** and c) **MC18**. Adapted with permission.[179] Copyright 2017, American Chemical Society. d) Absorption spectra of **MC17** (blue solid), **MC18** (orange solid), and **MC19** (red solid) in aggregate thin films. Dyes **MC17** (black dashed), **MC18** (black dotted), and **MC19** (black solid) show almost identical monomeric absorption spectra in solution. Adapted with permission.[187] Copyright 2018, Wiley-VCH. e) *EQE* spectra of PHJ OPDs based on **MC17**:**MC19** mixed thin films. Adapted with permission.[188] Copyright 2021, Wiley-VCH.

is observed as illustrated for **SQ8** in Figure 15c. This leads to typical hypsochromically shifted narrow absorption bands that originate mainly from Coulomb coupling (H-aggregates).[190]

In the solid state, however, often slip-stacked packing motifs are favored where donor and acceptor parts of the π-stacked chromophores are in close contact with each other (Figure 4). Here, subtle differences in the packing arrangement may lead to spectra that are either dominated by $J_{Coulomb}$ (conventional J-aggregate) or by CT-coupled J-aggregation, latter possibly even with an H-type $J_{Coulomb}$ component. Only recently has the interplay of these different types of coupling been properly interpreted from a theoretical point of view[48] and experimentally confirmed for **Bis-SQ1** whose self-assembly in solution can provide two distinct polymorphs by the applied cooling-rate that are characterized by entirely different absorption bands (Figure 15d).[50] For an aggregate with a nanotubular structure, a panchromatic absorption band with hypsochromically shifted maximum at 608 nm is observed that can only be explained by consideration of strong CT interactions between the aggregated chromophores. Accordingly, the pronounced hypsochromically shifted main absorption band should not be solely interpreted as an H-aggregate. Likewise, the other aggregate with nanosheet structure with head-to-tail packing arrangement and narrow bathochromically shifted absorption band should not be classified as a conventional J-aggregate despite its red-shifted narrow absorption band because also for this arrangement CT interactions contribute strongly to the spectral shift.

Based on these recent insights, some of the previously deduced packing models derived from aggregate and thin film spectra for squaraine dyes based purely on $J_{Coulomb}$, i.e., Kasha's exciton model, accordingly be erroneous. For instance, a variety of spin-coated thin films of squaraine dyes with both hypsochromically and bathochromically shifted absorption spectra or strongly broadened bands have been interpreted by the coexistence of H- and J-aggregate polymorphs but might now be attributed to a single aggregate species characterized by strong CT coupling.[191–195] With these new insights, the interpretation of the optical properties of squaraine aggregates is more demanding. Likewise, because subtle differences in packing could have a large impact on CT couplings, it is challenging to tailor specific optical properties in the thin film toward single-wavelength selective photodetectors by supramolecular engineering for squaraine dyes. Nevertheless and in particular for NIR photodetectors, squaraine dyes have great potential because their absorption properties can be easily tuned toward longer wavelengths (see Figure 15b) by suitable heterocyclic donor units from 4-methylquinolinium (**SQ1**) or naphtolactame (**SQ9** and **SQ10**) derived enamine bases. **Figure 16** gives an

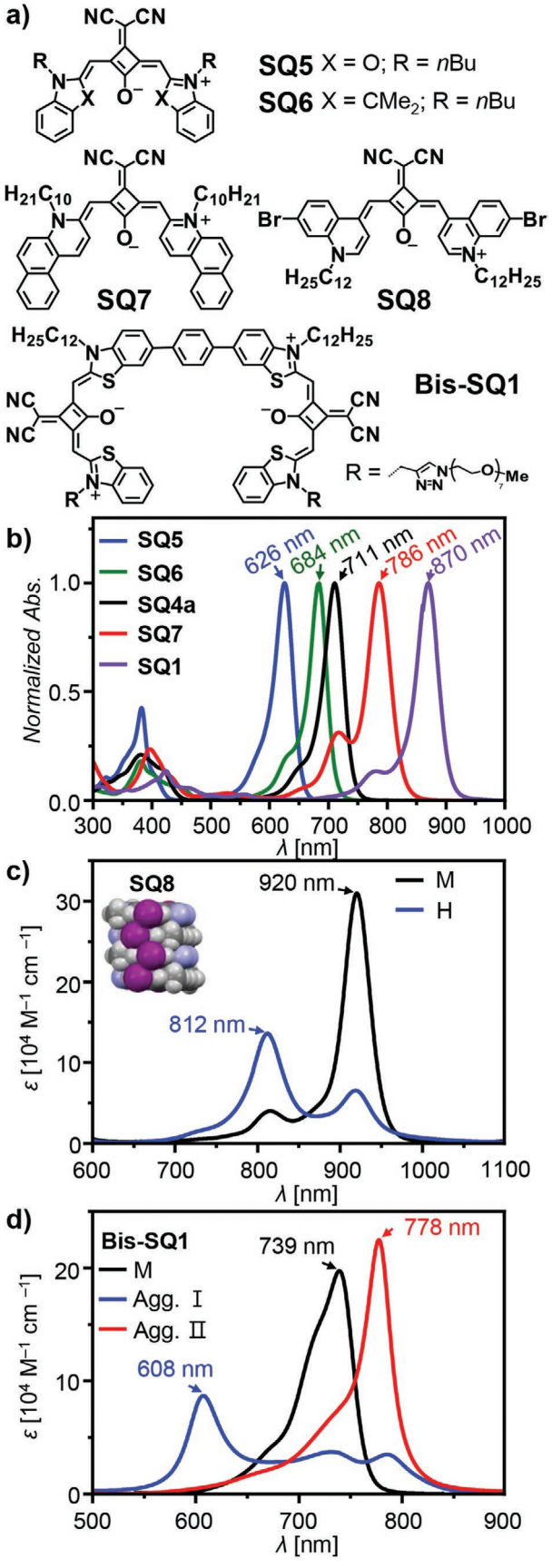

overview of the structures of squaraine dyes that have been successfully utilized in efficient OPDs and their respective device properties are listed in **Table 5**.

As to be expected based on these new insights into the intermolecular interactions between squaraine dyes, most squaraine-based materials show a rather broad and unselective NIR spectral photoresponse within the active layers of OPDs, despite the sharp and intense absorption spectra of monomers in solution (Section 3.1). Nevertheless, as we will show in the following, their incorporation in photodetectors within the last decade afforded quite impressive results.[196–198] In their endeavor to push the absorption range beyond the 1000 nm threshold, Hany and co-workers demonstrated several NIR-absorbing OPDs of squaraine dyes **SQ9** and **SQ10** that are equipped with naphtholactame-derived benz[*c*,*d*]indolium donor units. Indeed with these donor units, absorption maxima of 882 nm (**SQ9**) and 935 nm (**SQ10**) were reached for monomers, which further shifted to 995 nm (**SQ10**) in the thin film.[199,200] However, because either amorphous layers or only weakly interacting chromophores are present in these materials, no high wavelength selectivity could be achieved which resulted in $FWHM_{EQE}$ values above 200 nm. Although a photoresponse bandwidth of about 100 nm with broadband absorbing and amorphous squaraines (**SQ11–13**) has been demonstrated using an optical cavity effect, such device structures require a precisely controlled active layer thickness making them again inapplicable for future stacked device architectures (Figure 10).[201–203]

The large longitudinal displacement without an intermolecular overlap of donor and acceptor moieties in the crystal structure seems to alleviate the spectral broadening in thin film state. **SQ14** is one of the earliest reported squaraine dyes, and its intense monomeric absorption in the NIR ($\varepsilon = 1.32 \times 10^5$ mol^{-1} cm^{-1}, $\lambda_{max} = 770$ nm in $CHCl_3$) has already been described in 1966.[204] In their research on NIR phototransistors, Anthopoulos and co-workers reported that **SQ14** forms slipped stacks ($\Theta \approx 20°$) in a co-facial herringbone structure, and that the annealed thin film exhibits a strongly bathochromically shifted absorption maximum at 925 nm with a half-width at half-maximum of less than 50 nm (approximated $FWHM < 100$ nm).[205] While some residual absorption of the annealed layer remained in the visible light region, the crystal structure and the 150 nm red-shifted absorption of the annealed thin film strongly imply that **SQ14** indeed forms $J_{Coulomb}$-dominated J-aggregates in thin films. In contrast to this work, Hayden and co-workers could only report a broad photospectral response based on an **SQ14**:$PC_{61}BM$ BHJ OPD with an *EQE* of about 20% and an $FWHM_{EQE} > 200$ nm at around $\lambda_{max,EQE} = 800$ nm, presumably due to a more amorphous layer in which **SQ14** mainly retains its monomer-like absorption properties.[206] Likewise, **SQ15** shows a slipped-stacked packing arrangement ($\Theta \approx 20°$)

Figure 15. a) Chemical structures of representative squaraine dyes. b) Absorption spectra of various squaraine dyes in solution. Adapted with permission.[84] Copyright 2014, American Chemical Society. Adapted with permission.[189] Copyright 2013, Wiley-VCH. c) Absorption spectra of **SQ8** in its monomeric and its (not fully) aggregated state. Adapted with permission.[190] Copyright 2012, Wiley-VCH. d) Absorption spectra of **Bis-SQ1** in its monomeric and in two different aggregated states. Adapted with permission.[50] Copyright 2021, Wiley-VCH.

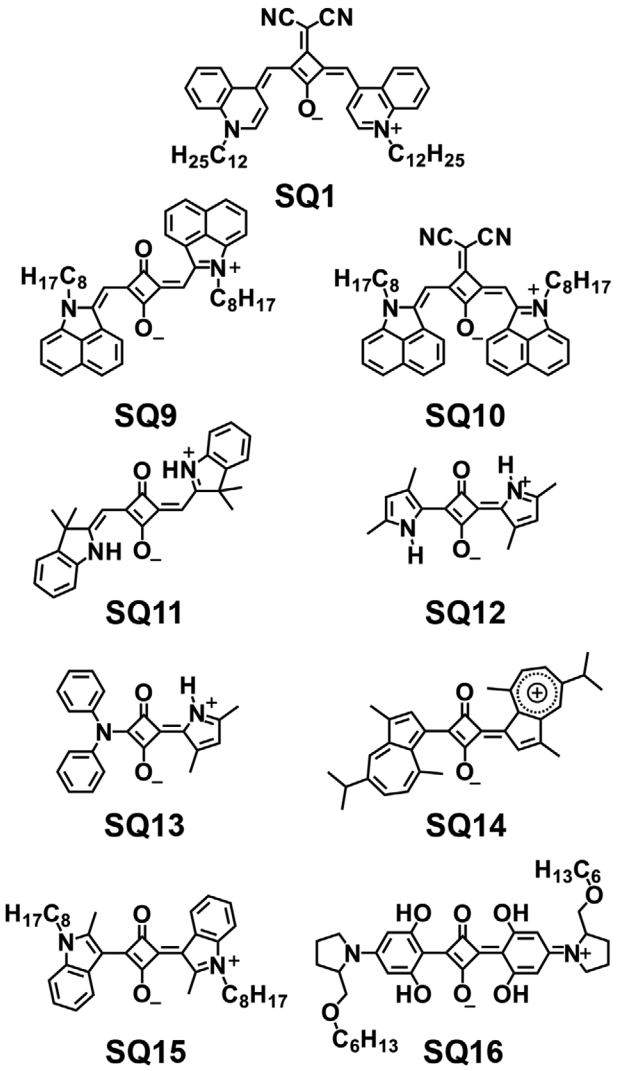

Figure 16. Molecular structures of squaraine dyes.

in the single crystal, and exhibits a bathochromically shifted absorption spectrum with an *FWHM* of less than 150 nm in the thin film.[207] Accordingly, Natali and co-workers reported **SQ15**:$PC_{61}BM$ BHJ thin-film OPDs with an *EQE* of 12% and an $FWHM_{EQE}$ of about 150 nm at $\lambda_{max,EQE}$ = 590 nm.[208]

Different from the above-mentioned materials, two distinctive hypsochromically and bathochromically shifted absorption bands are observable for the crystalline thin films of **SQ16** and **SQ1**. The special bis(aniline)-donor-based squaraine dyes bearing four hydrogen-bonding and thereby planarity-enforcing hydroxyl groups have already been discussed in Section 3.1 as they can provide highly efficient OSCs. For the detection of circularly polarized light by OPDs, Schiek and co-workers equipped this chromophore with enantiomerically pure prolinol substituents (**SQ16**).[193,194] According to their in-depth studies, pristine-annealed spin-coated films of **SQ16** exhibit both hypsochromically and bathochromically shifted absorption bands at 545 and 750 nm, respectively, which were attributed to the presence of polymorphs but could also originate from CT coupling within a single polymorph as discussed above. Without the annealing process, the thin film of **SQ16** showed an H-type dominant narrow absorption band[193] with an *FWHM* of less than 100 nm at λ_{max} = 545 nm.[194] Unfortunately, this interesting band did not show up in **SQ16**:$PC_{61}BM$ BHJ layers where the OPD exhibits a broad photospectral response (*EQE* = 50%; $FWHM_{EQE}$ of about 150 nm at $\lambda_{max,EQE}$ = 530 nm).

Most recently, such a narrow-band photospectral absorption in the NIR range has successfully been achieved by our group based on aggregates of dipolar **SQ1**, with monomer absorption maximum at 876 nm.[49] Similar to the previously mentioned amorphous squaraine dyes, as-cast **SQ1** thin film shows a broadband and only slightly red-shifted absorption spectrum in the red to NIR region with *FWHM* > 200 nm. In our view, this red-shift can be attributed to the effect of the surrounding matrix for such highly polarizable dipolar chromophores and does not indicate any specific intermolecular coupling, neither from $J_{Coulomb}$ nor CT-coupled J-aggregation. However, after a thermal annealing process, the crystalline thin

Table 5. Optical and device properties of OPDs based on squaraine dyes.

Materials	Optical[a]		Device[b]							Ref.
	λ_{max} [nm]	*FWHM* [nm]	$\lambda_{max,EQE}$ [nm]	$FWHM_{EQE}$ [nm]	*EQE*(@ V_{bias}) [%]	*R* [mA W^{-1}]	D^*_{max} [10^{11} Jones]	f_{-3dB} [kHz]	Active layer	
SQ1	1040	71	1050	85	12 (@ 0 V)	102	0.4	300	BHJ	[49]
SQ9	970	250[c]	980	250[c]	84 (@ −10 V)	664[d]	–	–	BHJ	[199]
SQ10	995	200[c]	1025	250[c]	33 (@ −8 V)	273[d]	–	–	BHJ	[200]
SQ11	690[a]	120[c]	680	80	15 (@ −2 V)	82[d]	32	190	SL	[201]
SQ12	600	135	600	110	66 (@ −2 V)	319[d]	77	–	SL	[202]
SQ13	500[a]	99	500	90	16 (@ −3 V)	65[d]	1	–	SL	[203]
SQ14	–	–	800[a]	250[c]	20 (@ −2 V)[a]	129[d]	–	100	BHJ	[206]
SQ15	600[a]	130[c]	590	150[c]	12 (@ −1 V)	57[d]	–	–	BHJ	[208]
SQ16	545	70[c]	530[c]	150[c]	50 (@ 0 V)[a]	214[d]	–	–	BHJ	[194]

[a]The wavelength absorption maximum (λ_{max}) and its *FWHM* in the neat thin film; [b]The *EQE* maximum wavelength ($\lambda_{max,EQE}$) and its *FWHM* ($FWHM_{EQE}$) in the thin film device. Active layer: single-layer (SL); [c]Values were estimated from the graphical data provided in the literature; [d]Values were estimated according to Equation (3).

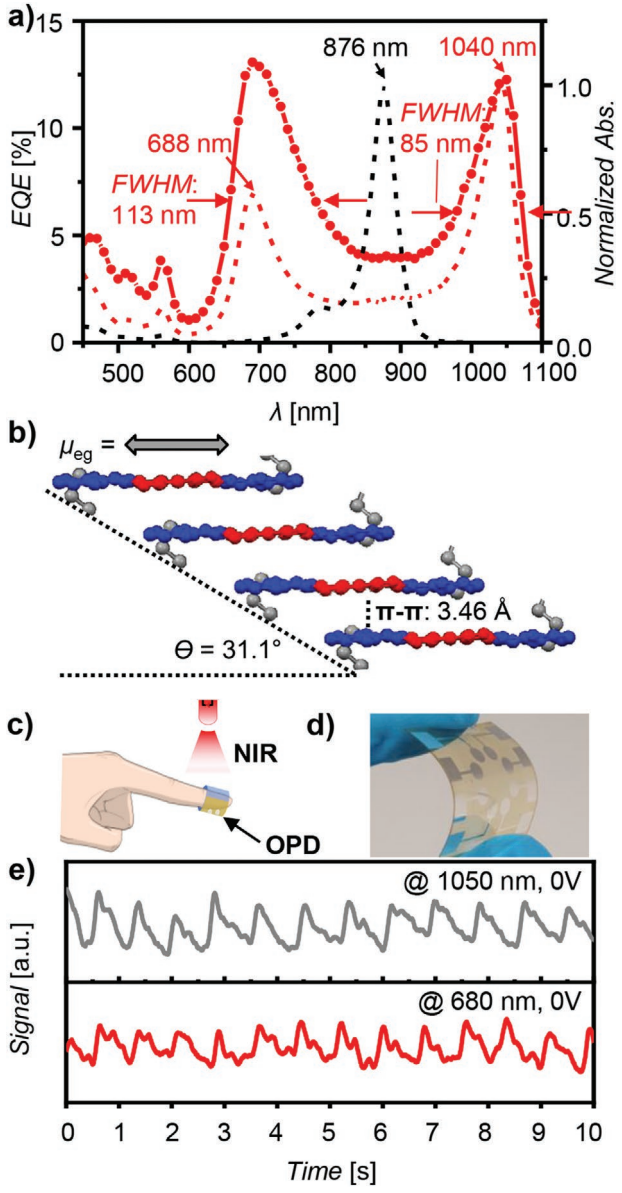

Figure 17. a) *EQE* spectrum of **SQ1**:$PC_{61}BM$ BHJ OPD (red connected circle symbol) and absorption spectra of **SQ1** in solution (black dashed) and in thin film (red dashed). b) The slip-stacked packing arrangement of **SQ1** in the single crystal. c) Schematic illustration of a photoplethysmogram (PPG) sensing device. d) Photographs of a flexible **SQ1** OPD and e) the PPG sensor demonstration using the **SQ1**-based device. Adapted with permission.[49] Copyright 2021, Wiley-VCH.

film shows two distinct absorption bands, each one hypsochromically and bathochromically shifted at 688 and 1040 nm (**Figure 17**a) with very narrow *FWHM* of 65 nm (1335 cm^{-1}) and 59 nm (555 cm^{-1}), respectively. The single-crystal structure demonstrates that **SQ1** molecules experience intimate π–π contact (3.46 Å) with large overlap of the donor and acceptor moieties in a slip-stacked packing arrangement (Θ = 31.1°, Figure 17b), which enabled enhanced charge carrier mobility. Based on theoretical calculations, the band splitting of the **SQ1** thin-film spectrum originates from CT-coupled J-aggregation. This unique optical property allows for a BHJ OPD with $PC_{61}BM$ with dual narrowband selectivity in the red as well as NIR spectral region, exhibiting an *EQE* of 13% with $FWHM_{EQE}$ = 113 nm at $\lambda_{max,EQE}$ = 690 nm as well as an *EQE* of 12% with $FWHM_{EQE}$ = 85 nm at $\lambda_{max,EQE}$ = 1050 nm at 0 V sample bias, respectively (Figure 17a). With the successful heart-rate monitoring in a transmission mode photoplethysmography application with flexible OPDs based on **SQ1**, the advantage of selective excitation by tissue penetrating NIR light was demonstrated (Figure 17c–e).

5. Summary and Future Perspectives

During the last two decades, our knowledge about dye aggregates has significantly improved. This includes insights into the noncovalent interactions that influence the self-assembly of dye molecules in solution,[209] their favored packing arrangements in the solid state, as well as the comprehension of the electronic interactions among the dyes in their aggregates that affect the functional properties of the material.[7,41] In this review, our focus was on the important class of slip-stacked dye aggregates with red-shifted absorption bands that are typically called J-aggregates. Because a significant fraction of recently published articles applied the name J-aggregates to materials that do not exhibit red-shifted absorption bands originating from negative Coulomb coupling, thereby being at odds with the definition of J-aggregates based on Kasha's molecular exciton theory, the different electronic interactions leading to red-shifted absorption bands were outlined first in Section 2 of this review. Based on our clarifications, we suggest distinguishing conventional J-aggregates whose red-shifts are due to long-range Coulomb interactions (classical exciton coupling) from CT-J-aggregates where the major contribution to the red-shift originates from short-range orbital interactions.

The prevailing interaction is indeed strongly dependent on the mutual arrangement of the dyes in the aggregate and the type of chromophore. Thus, most cyanine and merocyanine dyes exhibit classical J-aggregation dominated by Coulomb coupling. Perylene bisimides often form CT-mediated J-aggregates, while for squaraine dyes additional CT-coupling J-aggregation is often prevalent. Depending on the mutual packing arrangement, the contributions of these intermolecular couplings appear to vary in aggregates of acceptor–donor–acceptor (A-D-A) dyes that constitute the currently most successful class of NFA materials for bulk heterojunction OSCs. Indeed, as revealed by our analysis of absorption spectra in particular for J-aggregate-forming squaraine and A-D-A dyes, CT couplings governed by HOMO–HOMO and LUMO–LUMO interactions are beneficial for solar light harvesting both with regard to optical properties, i.e., red-shifted absorption bands, as well as electronic properties, i.e., charge carrier transport. It is also noted that the admixture of different couplings leads to band broadening as desired for panchromatic light absorption in organic photovoltaics.

While the photoactive layers and devices utilized for OPDs can be quite similar to those utilized for panchromatic OSCs, for the former narrow bandwidths are desirable. Accordingly, a set of functional dyes is needed that covers with their narrow bands the spectral range from the UV via the visible (blue,

green, red) up to the NIR, similar as for photosensitizers used in silver halide photography in old times. As we could show in this review such narrow bandwidths in the visible spectral range are most favorably accomplished by cyanine and merocyanine dye aggregates for which the electronic interactions are governed by long-range Coulomb couplings with concomitant exchange narrowing. As demonstrated in particular for merocyanine dyes, similarly high photocurrents can be accomplished for H- and J-aggregates, which is highly beneficial for narrow bandwidth detectors covering the visible range. Accordingly, face-to-face stacked H-aggregates are ideal for the blue spectral range while slip-stacked J-aggregates are most suited for the red spectral range. For the NIR spectral range, squaraine dye aggregates are particularly promising, in particular if recent insights into the strong influence of CT-coupled J-aggregation for specific packing arrangements is taken into consideration in the materials design. It is rather impressive that some of the presented OPDs can already compete with their commercially available counterparts based on inorganic materials. Indeed, with the demonstrated portfolio of already successfully established (ultra)-narrowband OPDs based on merocyanine and squaraine aggregates with specific absorption spectra ranging from 480 to 1050 nm and $FWHM_{EQE}$ well below 100 nm, the envisioned realization of multispectral and hyperspectral imaging sensing (Figure 10b) comprised by multiple stacked narrowband photodetectors in a compact device architecture might soon become reality.

It is our firm conviction that the insights into dye–dye interactions acquired during the last years will also have a strong impetus on the development of organic materials for optoelectronics beyond the two applications discussed in this review. Here, it will be important to understand which particular couplings are most beneficial for the respective functional properties that may include exciton migration, hole or electron transport, population of multiexciton states for singlet fission, chiroptical and spin-dependent properties as well as fluorescence or phosphorescence. The often multifunctional demands for the respective aggregated materials might be accomplished by tailored derivatives of the here discussed dyes that indeed constitute prototypes for the design of functional materials properties by consideration of both molecular and supramolecular engineering concepts. Ingenious chemists may, however, also identify other dyes whose supramolecular engineering endorses desirable functional properties. For instance, the recent successful supramolecular engineering of fluorescent J-aggregates from BODIPY dyes appears like an interesting starting point toward a new class of highly emissive solid-state materials.[210,211] Likewise, research on room-temperature phosphorescence has gained significant momentum but has not yet identified the most suitable supramolecular packing motifs for the efficient population of triplet states by spin–orbit coupling.[212] Further, motivated by prospects of circularly polarized luminescence[213] and spin-selective transport phenomena,[214] tailored aggregates composed of chiral π-scaffolds are interesting for being explored as chiroptical materials.[215,216] Such novel tailored materials will provide an impetus for the realization of long time desired organic lasers[217,218] as well as for entirely new devices in the areas of microcavity photonics,[219] for sensing applications,[220] or for spin-selective charge transport.[221]

Acknowledgements

J.H.K. and T.S. contributed equally to this work. The authors thank Prof. Jürgen Köhler (Bayreuth) and Dr. Heinz Mustroph (Dessau) for helpful advice. Financial support from the Bavarian State Ministry for Science and the Arts for the research program "Solar Technologies Go Hybrid" and the Key Lab for Supramolecular Polymers of the Bavarian Polymer Institute is gratefully acknowledged.

Open access funding enabled and organized by Projekt DEAL.

Conflict of Interest

The authors declare no conflict of interest.

Keywords

crystal engineering, exciton coupling, J-aggregates, organic photodiodes, organic solar cells

Received: June 18, 2021
Revised: August 16, 2021
Published online: October 19, 2021

[1] J. R. Lakowitz, *Principles of Fluorescence Spectroscopy*, 3rd ed., Springer, New York **2006**.
[2] A. Hagfeldt, G. Boschloo, L. Sun, L. Kloo, H. Pettersson, *Chem. Rev.* **2010**, *110*, 6595.
[3] A. P. H. J. Schenning, E. W. Meijer, *Chem. Commun.* **2005**, 3245.
[4] F. Würthner, K. Meerholz, *Chem. - Eur. J.* **2010**, *16*, 9366.
[5] Z. B. Henson, K. Müllen, G. C. Bazan, *Nat. Chem.* **2012**, *4*, 699.
[6] J. Gierschner, S. Y. Park, *J. Mater. Chem. C* **2013**, *1*, 5818.
[7] D. Bialas, E. Kirchner, M. I. S. Röhr, F. Würthner, *J. Am. Chem. Soc.* **2021**, *143*, 4500.
[8] R. M. Young, M. R. Wasielewski, *Acc. Chem. Res.* **2020**, *53*, 1957.
[9] F. Würthner, C. R. Saha-Möller, B. Fimmel, S. Ogi, P. Leowanawat, D. Schmidt, *Chem. Rev.* **2016**, *116*, 962.
[10] A. Köhler, H. Bässler, *Electronic Processes in Organic Semiconductors*, Wiley-VCH, Weinheim, Germany **2015**.
[11] A. Zampetti, A. Minotto, F. Cacialli, *Adv. Funct. Mater.* **2019**, *29*, 1807623.
[12] F. Würthner, T. E. Kaiser, C. R. Saha-Möller, *Angew. Chem., Int. Ed.* **2011**, *50*, 3376; *Angew. Chem.* **2011**, *123*, 3436.
[13] S. D. Dimitrov, J. R. Durrant, *Chem. Mater.* **2014**, *26*, 616.
[14] O. Ostroverkhova, *Chem. Rev.* **2016**, *116*, 13279.
[15] A. Karki, A. J. Gillett, R. H. Friend, T.-Q. Nguyen, *Adv. Energy Mater.* **2021**, *11*, 2003441.
[16] X. Liu, B. P. Rand, S. R. Forrest, *Trends Chem.* **2019**, *1*, 815.
[17] a) E. E. Jelley, *Nature* **1936**, *138*, 1009; b) E. E. Jelley, *Nature* **1937**, *139*, 631.
[18] a) G. Scheibe, *Angew. Chem.* **1936**, *49*, 563; b) G. Scheibe, *Angew. Chem.* **1937**, *50*, 75; c) G. Scheibe, L. Kandler, H. Ecker, *Naturwissenschaften* **1937**, *25*, 75; d) G. Scheibe, *Angew. Chem.* **1937**, *50*, 212.
[19] A. H. Herz, *Photogr. Sci. Eng.* **1974**, *18*, 323.
[20] S. Fujita, *Organic Chemistry of Photography*, Springer, Berlin, Germany **2004**.
[21] M. Gill, H. Mustroph, *Chem. Unserer Zeit* **2015**, *49*, 124.
[22] H. Mustroph, *Phys. Sci. Rev.* **2020**, *5*, 20190145.
[23] A. H. Herz, *Adv. Colloid Interface Sci.* **1977**, *8*, 237.
[24] S. Makio, N. Kanamaru, J. Tanaka, *Bull. Chem. Soc. Jpn.* **1980**, *53*, 3120.

[25] T. E. Kaiser, V. Stepanenko, F. Würthner, *J. Am. Chem. Soc.* **2009**, *131*, 6719.
[26] D. Zhao, J. S. Moore, *Org. Biomol. Chem.* **2003**, *1*, 3471.
[27] M. Wehner, F. Würthner, *Nat. Chem. Rev.* **2020**, *4*, 38.
[28] F. Würthner, *Angew. Chem., Int. Ed.* **2020**, *59*, 14192; *Angew. Chem.* **2020**, *132*, 14296.
[29] Y. Hong, J. W. Y. Lam, B. Z. Tang, *Chem. Soc. Rev.* **2011**, *40*, 5361.
[30] J. L. Bricks, Y. L. Slominskii, I. D. Panas, A. P. Demchenko, *Methods Appl. Fluoresc.* **2018**, *6*, 012001.
[31] B.-K. An, S.-K. Kwon, S.-D. Jung, S. Y. Park, *J. Am. Chem. Soc.* **2002**, *124*, 14410.
[32] T. Brixner, R. Hildner, J. Köhler, C. Lambert, F. Würthner, *Adv. Energy Mater.* **2017**, *7*, 1700236.
[33] M. Kasha, H. R. Rawls, M. A. El-Bayoumi, *Pure Appl. Chem.* **1965**, *11*, 371.
[34] S. Kirstein, S. Daehne, *Int. J. Photoenergy* **2006**, *2006*, 20363.
[35] C. Didraga, J. A. Klugkist, J. Knoester, *J. Phys. Chem. B* **2002**, *106*, 11474.
[36] T. Mirkovic, E. E. Ostroumov, J. M. Anna, R. van Grondelle, Govindjee, G. D. Scholes, *Chem. Rev.* **2017**, *117*, 249.
[37] C. Didraga, J. Knoester, *J. Lumin.* **2004**, *110*, 239.
[38] V. I. Prokhorenko, D. B. Steensgaard, A. R. Holzwarth, *Biophys. J.* **2003**, *85*, 3173.
[39] R. J. Cogdell, J. Köhler, in *Quantum Efficiency in Complex Systems, Part I: Biomolecular Systems*, Vol. *83* (Eds: E. R. Weber, M. Thorwart, U. Würfel), Academic Press, San Diego **2010**, pp. 77–94.
[40] V. Huber, S. Sengupta, F. Würthner, *Chem. - Eur. J.* **2008**, *14*, 7791.
[41] N. J. Hestand, F. C. Spano, *Chem. Rev.* **2018**, *118*, 7069.
[42] N. J. Hestand, F. C. Spano, *J. Chem. Phys.* **2015**, *143*, 244707.
[43] C. Kaufmann, D. Bialas, M. Stolte, F. Würthner, *J. Am. Chem. Soc.* **2018**, *140*, 9986.
[44] F. C. Spano, C. Silva, *Annu. Rev. Phys. Chem.* **2014**, *65*, 477.
[45] A. Oleson, T. Zhu, I. S. Dunn, D. Bialas, Y. Bai, W. Zhang, M. Dai, D. R. Reichman, R. Tempelaar, L. Huang, F. C. Spano, *J. Phys. Chem. C* **2019**, *123*, 20567.
[46] M. Hecht, F. Würthner, *Acc. Chem. Res.* **2021**, *54*, 642.
[47] J. Mizuguchi, K. Tojo, *J. Phys. Chem. B* **2002**, *106*, 767.
[48] N. J. Hestand, C. Zheng, A. R. Penmetcha, B. Cona, J. A. Cody, F. C. Spano, C. J. Collison, *J. Phys. Chem. C* **2015**, *119*, 18964.
[49] J. H. Kim, A. Liess, M. Stolte, A.-M. Krause, V. Stepanenko, C. Zhong, D. Bialas, F. Spano, F. Würthner, *Adv. Mater.* **2021**, *33*, 2100582.
[50] C.-A. Shen, D. Bialas, M. Hecht, V. Stepanenko, K. Sugiyasu, F. Würthner, *Angew. Chem., Int. Ed.* **2021**, *60*, 11949; *Angew. Chem.* **2021**, *133*, 12056.
[51] S. Sanyal, A. Painelli, S. K. Pati, F. Terenziani, C. Sissa, *Phys. Chem. Chem. Phys.* **2016**, *18*, 28198.
[52] F. C. Spano, *J. Am. Chem. Soc.* **2009**, *131*, 4267.
[53] F. C. Spano, *Acc. Chem. Res.* **2010**, *43*, 429.
[54] P. Cheng, Y. Yang, *Acc. Chem. Res.* **2020**, *53*, 1218.
[55] L. Dou, J. You, Z. Hong, Z. Xu, G. Li, R. A. Street, Y. Yang, *Adv. Mater.* **2013**, *25*, 6642.
[56] Y. Li, G. Xu, C. Cui, Y. Li, *Adv. Energy Mater.* **2018**, *8*, 1701791.
[57] Q. Liu, Y. Jiang, K. Jin, J. Qin, J. Xu, W. Li, J. Xiong, J. Liu, Z. Xiao, K. Sun, S. Yang, X. Zhang, L. Ding, *Sci. Bull.* **2020**, *65*, 272.
[58] C. Yan, S. Barlow, Z. Wang, H. Yan, A. K.-Y. Jen, S. R. Marder, X. Zhan, *Nat. Rev. Mater.* **2018**, *3*, 18003.
[59] C. J. Traverse, R. Pandey, M. C. Barr, R. R. Lunt, *Nat. Energy* **2017**, *2*, 849.
[60] S.-Y. Chang, P. Cheng, G. Li, Y. Yang, *Joule* **2018**, *2*, 1039.
[61] M. Gsänger, J. H. Oh, M. Könemann, H. W. Höffken, A.-M. Krause, Z. Bao, F. Würthner, *Angew. Chem., Int. Ed.* **2010**, *49*, 740; *Angew. Chem.* **2010**, *122*, 752.
[62] J.-L. Brédas, J. E. Norton, J. Cornil, V. Coropceanu, *Acc. Chem. Res.* **2009**, *42*, 1691.
[63] B. Walker, A. B. Tamayo, X.-D. Dang, P. Zalar, J. H. Seo, A. Garcia, M. Tantiwiwat, T.-Q. Nguyen, *Adv. Funct. Mater.* **2009**, *19*, 3063.
[64] M. Más-Montoya, R. A. J. Janssen, *Adv. Funct. Mater.* **2017**, *27*, 1605779.
[65] T.-Y. Li, T. Meyer, Z. Ma, J. Benduhn, C. Körner, O. Zeika, K. Vandewal, K. Leo, *J. Am. Chem. Soc.* **2017**, *139*, 13636.
[66] T.-Y. Li, J. Benduhn, Z. Qiao, Y. Liu, Y. Li, R. Shivhare, F. Jaiser, P. Wang, J. Ma, O. Zeika, D. Neher, S. C. B. Mannsfeld, Z. Ma, K. Vandewal, K. Leo, *J. Phys. Chem. Lett.* **2019**, *10*, 2684.
[67] P. E. Hartnett, A. Timalsina, H. S. Matte, N. Zhou, X. Guo, W. Zhao, A. Facchetti, R. P. Chang, M. C. Hersam, M. R. Wasielewski, T. J. Marks, *J. Am. Chem. Soc.* **2014**, *136*, 16345.
[68] A. Nowak-Król, K. Shoyama, M. Stolte, F. Würthner, *Chem. Commun.* **2018**, *54*, 13763.
[69] Q. Zhao, J. Liu, H. Wang, M. Li, K. Zhou, H. Yang, Y. Han, *J. Mater. Chem. C* **2015**, *3*, 8183.
[70] A. Bourdick, M. Reichenberger, A. Stradomska, G. C. Bazan, T.-Q. Nguyen, A. Köhler, S. Gekle, *J. Phys. Chem. B* **2018**, *122*, 9191.
[71] A. Mishra, D. Popovic, A. Vogt, H. Kast, T. Leitner, K. Walzer, M. Pfeiffer, E. Mena-Osteritz, P. Bäuerle, *Adv. Mater.* **2014**, *26*, 7217.
[72] T. Kraus, S. Lucas, P. Wolff, A. Aubele, E. Mena-Osteritz, P. Bäuerle, *Chem. - Eur. J.* **2021**, *27*, 10913.
[73] M. B. Qarai, X. Chang, F. C. Spano, *J. Chem. Phys.* **2020**, *153*, 244901.
[74] X. Chang, M. B. Qarai, F. C. Spano, *J. Chem. Phys.* **2021**, *155*, 034905.
[75] G. Chen, H. Sasabe, T. Igarashi, Z. Hong, J. Kido, *J. Mater. Chem. A* **2015**, *3*, 14517.
[76] J. He, Y. J. Jo, X. Sun, W. Qiao, J. Ok, T.-i. Kim, Z. Li, *Adv. Funct. Mater.* **2021**, *31*, 2008201.
[77] Y. Chen, W. Zhu, J. Wu, Y. Huang, A. Facchetti, T. J. Marks, *Org. Photonics Photovoltaics* **2019**, *6*, 1.
[78] A. Venkateswararao, K.-T. Wong, *Bull. Chem. Soc. Jpn.* **2021**, *94*, 812.
[79] S. Sreejith, P. Carol, P. Chithra, A. Ajayaghosh, *J. Mater. Chem.* **2008**, *18*, 264.
[80] A. Ajayaghosh, P. Chithra, R. Varghese, K. P. Divya, *Chem. Commun.* **2008**, 969.
[81] M. Tian, M. Furuki, I. Iwasa, Y. Sato, L. S. Pu, S. Tatsuura, *J. Phys. Chem. B* **2002**, *106*, 4370.
[82] U. Mayerhöffer, K. Deing, K. Gruß, H. Braunschweig, K. Meerholz, F. Würthner, *Angew. Chem., Int. Ed.* **2009**, *48*, 8776; *Angew. Chem.* **2009**, *121*, 8934.
[83] A. Kokil, A. M. Poe, Y. Bae, A. M. Della Pelle, P. J. Homnick, P. M. Lahti, J. Kumar, S. Thayumanavan, *ACS Appl. Mater. Interfaces* **2014**, *6*, 9920.
[84] M. Gsänger, E. Kirchner, M. Stolte, C. Burschka, V. Stepanenko, J. Pflaum, F. Würthner, *J. Am. Chem. Soc.* **2014**, *136*, 2351.
[85] K. C. Deing, U. Mayerhöffer, F. Würthner, K. Meerholz, *Phys. Chem. Chem. Phys.* **2012**, *14*, 8328.
[86] G. Chen, H. Sasabe, W. Lu, X.-F. Wang, J. Kido, Z. Hong, Y. Yang, *J. Mater. Chem. C* **2013**, *1*, 6547.
[87] J. Wojtyk, A. McKerrow, P. Kazmaier, E. Buncel, *Can. J. Chem.* **1999**, *77*, 903.
[88] G. Chen, H. Sasabe, Z. Wang, X.-F. Wang, Z. Hong, Y. Yang, J. Kido, *Adv. Mater.* **2012**, *24*, 2768.
[89] G. Wei, S. Wang, K. Renshaw, M. E. Thompson, S. R. Forrest, *ACS Nano* **2010**, *4*, 1927.
[90] G. Wei, X. Xiao, S. Wang, J. D. Zimmerman, K. Sun, Y. V. Diev, M. E. Thompson, S. R. Forrest, *Nano Lett.* **2011**, *11*, 4261.
[91] G. Chen, Z. Ling, B. Wie, J. Zhang, Z. Hong, H. Sasabe, J. Kido, *Front. Chem.* **2018**, *6*, 412.

[92] J. D. Zimmerman, B. E. Lassiter, X. Xiao, K. Sun, A. Dolocan, R. Gearba, D. A. Vanden Bout, K. J. Stevenson, P. Wickramasinghe, M. E. Thompson, S. R. Forrest, *ACS Nano* **2013**, *7*, 9268.
[93] S. Wang, L. Hall, V. V. Diev, R. Haiges, G. Wie, X. Xiao, P. I. Djurovich, S. R. Forrest, M. E. Thompson, *Chem. Mater.* **2011**, *23*, 4789.
[94] G. Wei, X. Xiao, S. Wang, K. Sun, K. J. Bergemann, M. E. Thompson, S. R. Forrest, *ACS Nano* **2012**, *6*, 972.
[95] V. C. Nikolis, A. Mischok, B. Siegmund, J. Kublitski, X. Jia, J. Benduhn, U. Hörmann, D. Neher, M. C. Gather, D. Spoltore, K. Vandewal, *Nat. Commun.* **2019**, *10*, 3706.
[96] H. Lai, F. He, *Adv. Energy Mater.* **2020**, *10*, 2002678.
[97] D. Li, X. Zhang, D. Liu, T. Wang, *J. Mater. Chem. A* **2020**, *8*, 15607.
[98] Q. Zhao, H. Lai, H. Chen, H. Li, F. He, *J. Mater. Chem. A* **2021**, *9*, 1119.
[99] N. M. Kronenberg, M. Deppisch, F. Würthner, H. W. A. Lademann, K. Deing, K. Meerholz, *Chem. Commun.* **2008**, 6489.
[100] H. Bürckstümmer, E. V. Ttulyakova, M. Deppisch, M. R. Lenze, N. M. Kronenberg, M. Gsänger, M. Stolte, K. Meerholz, F. Würthner, *Angew. Chem., Int. Ed.* **2011**, *50*, 11628; *Angew. Chem.* **2011**, *123*, 11832.
[101] A. Arjona-Esteban, J. Krumrain, A. Liess, M. Stolte, L. Huang, D. Schmidt, V. Stepanenko, M. Gsänger, D. Hertel, K. Meerholz, F. Würthner, *J. Am. Chem. Soc.* **2015**, *137*, 13524.
[102] F. Würthner, S. Yao, J. Schilling, R. Wortmann, M. Redi-Abshiro, E. Mecher, F. Gallego-Gomez, K. Meerholz, *J. Am. Chem. Soc.* **2001**, *123*, 2810.
[103] A. Zitzler-Kunkel, M. R. Lenze, N. M. Kronenberg, A.-M. Krause, M. Stolte, K. Meerholz, F. Würthner, *Chem. Mater.* **2014**, *26*, 4856.
[104] A. Zitzler-Kunkel, M. R. Lenze, K. Meerholz, F. Würthner, *Chem. Sci.* **2013**, *4*, 2071.
[105] C. Poelking, M. Tietze, C. Elschner, S. Olthof, D. Hertel, B. Baumeier, F. Würthner, K. Meerholz, K. Leo, D. Andrienko, *Nat. Mater.* **2015**, *14*, 434.
[106] A. Mishra, M. L. Keshtov, A. Looser, R. Singhal, M. Stolte, F. Würthner, P. Bäuerle, G. D. Sharma, *J. Mater. Chem. A* **2017**, *5*, 14887.
[107] A. Nowak-Król, R. Wagener, F. Kraus, A. Mishra, P. Bäuerle, F. Würthner, *Org. Chem. Front.* **2016**, *3*, 545.
[108] F. Würthner, *Acc. Chem. Res.* **2016**, *49*, 868.
[109] H. Huang, L. Yang, A. Facchetti, T. J. Marks, *Chem. Rev.* **2017**, *117*, 1029.
[110] Y. Lin, J. Wang, Z.-G. Zhang, H. Bai, Y. Li, D. Zhu, X. Zhan, *Adv. Mater.* **2015**, *27*, 1170.
[111] T. J. Aldrich, M. Matta, W. Zhu, S. M. Swick, C. L. Stern, G. C. Schatz, A. Facchetti, F. S. Melkonyan, T. J. Marks, *J. Am. Chem. Soc.* **2019**, *141*, 3274.
[112] M. C. Heiber, K. Kister, A. Baumann, V. Dyakonov, C. Deibel, T.-Q. Nguyen, *Phys. Rev. Appl.* **2017**, *8*, 054043.
[113] O. Wodo, S. Tirthapura, S. Chaudhary, B. Ganapathysubramanian, *J. Appl. Phys.* **2012**, *112*, 064316.
[114] Y. Firdaus, V. M. Le Corre, S. Karuthedath, W. Liu, A. Markina, W. Huang, S. Chattopadhyay, M. M. Nahid, M. I. Nugraha, Y. Lin, A. Seitkhan, A. Basu, W. Zhang, I. McCulloch, H. Ade, J. Labram, F. Laquai, D. Andrienko, L. J. A. Koster, T. D. Anthopoulos, *Nat. Commun.* **2020**, *11*, 5220.
[115] Y.-X. Zhang, J. Fang, W. Li, Y. Shen, J.-D. Chen, Y. Li, H. Gu, S. Pelivani, M. Zhang, Y. Li, J.-X. Tang, *ACS Nano* **2019**, *13*, 4686.
[116] Y. Yang, Z.-G. Zhang, H. Bin, S. Chen, L. Gao, L. Xue, C. Yang, Y. Li, *J. Am. Chem. Soc.* **2016**, *138*, 15011.
[117] X. Li, H. Huang, I. Angunawela, J. Zhou, J. Du, A. Liebman-Pelaez, C. Zhu, Z. Zhang, L. Meng, Z. Xie, H. Ade, Y. Li, *Adv. Funct. Mater.* **2020**, *30*, 1906855.
[118] Z. Xiao, X. Jia, D. Li, S. Wang, X. Geng, F. Liu, J. Chen, S. Yang, T. P. Russell, L. Ding, *Sci. Bull.* **2017**, *62*, 1494.
[119] W. Li, M. Chen, J. Cai, E. L. K. Spooner, H. Zhang, R. S. Gurney, D. Liu, Z. Xiao, D. G. Lidzey, L. Ding, T. Wang, *Joule* **2019**, *3*, 819.
[120] J. Yuan, Y. Zhang, L. Zhou, G. Zhang, H.-L. Yip, T.-K. Lau, X. Lu, C. Zhu, H. Peng, P. A. Johnson, M. Leclerc, Y. Cao, J. Ulanski, Y. Li, Y. Zou, *Joule* **2019**, *3*, 1140
[121] X. Li, H. Lu, W. Zhu, *ChemPlusChem* **2021**, *86*, 700.
[122] W. Zhu, A. P. Spencer, S. Mukherjee, J. M. Alzola, V. K. Sangwan, S. H. Amsterdam, S. M. Swick, L. O. Jones, M. C. Heiber, A. A. Herzing, G. Li, C. L. Stern, D. M. DeLongchamp, K. L. Kohlstedt, M. C. Hersam, G. C. Schatz, M. R. Wasielewski, L. X. Chen, A. Facchetti, T. J. Marks, *J. Am. Chem. Soc.* **2020**, *142*, 14532.
[123] C. Xiao, C. Li, F. Liu, L. Zhang, W. Li, *J. Mater. Chem. C* **2020**, *8*, 5370.
[124] G. Zhang, X.-K. Chen, J. Xiao, P. C. Y. Chow, M. Ren, G. Kupgan, X. Jiao, C. C. S. Chan, X. Du, R. Xia, Z. Chen, J. Yuan, Y. Zhang, S. Zhang, Y. Liu, Y. Zou, H. Yan, K. S. Wong, V. Coropceanu, N. Li, C. J. Brabec, J.-L. Bredas, H.-L. Yip, Y. Cao, *Nat. Commun.* **2020**, *11*, 3943.
[125] S. M. Swick, W. Zhu, M. Matta, T. J. Aldrich, A. Harbuzaru, J. T. Lopez Navarrete, R. Ponce Ortiz, K. L. Kohlstedt, G. C. Schatz, A. Facchetti, F. S. Melkonyan, T. J. Marks, *Proc. Natl. Acad. Sci. U. S. A.* **2018**, *115*, E8341.
[126] V. Coropceanu, X.-K. Chen, T. Wang, Z. Zheng, J.-L. Brédas, *Nat. Rev. Mater.* **2019**, *4*, 689.
[127] G. Han, T. Hu, Y. Yi, *Adv. Mater.* **2020**, *32*, 2000975.
[128] D. Qian, Z. Zheng, H. Yao, W. Tress, T. R. Hopper, S. Chen, S. Li, J. Liu, S. Chen, J. Zhang, X.-K. Liu, B. Gao, L. Ouyang, Y. Jin, G. Pozina, I. A. Buyanova, W. M. Chen, O. Inganäs, V. Coropceanu, J.-L. Bredas, H. Yan, J. Hou, F. Zhang, A. A. Bakulin, F. Gao, *Nat. Mater.* **2018**, *17*, 703.
[129] F. D. Eisner, M. Azzouzi, Z. Fei, X. Hou, T. D. Anthopoulos, T. J. S. Dennis, M. Heeney, J. Nelson, *J. Am. Chem. Soc.* **2019**, *141*, 6362.
[130] J. Liu, S. Chen, D. Qian, B. Gautam, G. Yang, J. Zhao, J. Bergqvist, F. Zhang, W. Ma, H. Ade, O. Inganäs, K. Gundogdu, F. Gao, H. Yan, *Nat. Energy* **2016**, *1*, 16089.
[131] L. Perdigón-Toro, L. Q. Phuong, S. Zeiske, K. Vandewal, A. Armin, S. Shoaee, D. Neher, *ACS Energy Lett.* **2021**, *6*, 557.
[132] V. Pecunia, *Organic Narrowband Photodetectors: Materials, Devices and Applications*, Institute Of Physics Publishing, Bristol, UK **2019**.
[133] R. D. Jansen-van Vuuren, A. Armin, A. K. Pandey, P. L. Burn, P. Meredith, *Adv. Mater.* **2016**, *28*, 4766.
[134] P. C. Y. Chow, T. Someya, *Adv. Mater.* **2020**, *32*, 1902045.
[135] V. Pecunia, *J. Phys. Mater.* **2019**, *2*, 042001.
[136] C. Wang, X. Zhang, W. Hu, *Chem. Soc. Rev.* **2020**, *49*, 653.
[137] M. Biele, C. Montenegro Benavides, J. Hürdler, S. F. Tedde, C. J. Brabec, O. Schmidt, *Adv. Mater. Technol.* **2019**, *4*, 1800158.
[138] L. Zhang, T. Yang, L. Shen, Y. Fang, L. Dang, N. Zhou, X. Guo, Z. Hong, Y. Yang, H. Wu, J. Huang, Y. Liang, *Adv. Mater.* **2015**, *27*, 6496.
[139] C. Fuentes-Hernandez, W.-F. Chou, T. M. Khan, L. Diniz, J. Lukens, F. A. Larrain, V. A. Rodriguez-Toro, B. Kippelen, *Science* **2020**, *370*, 698.
[140] J. Huang, J. Lee, J. Vollbrecht, V. V. Brus, A. L. Dixon, D. X. Cao, Z. Zhu, Z. Du, H. Wang, K. Cho, G. C. Bazan, T.-Q. Nguyen, *Adv. Mater.* **2020**, *32*, 1906027.
[141] Y. Chen, Y. Zheng, Y. Jiang, H. Fan, X. Zhu, *J. Am. Chem. Soc.* **2021**, *143*, 4281.
[142] A. Armin, R. D. Jansen-van Vuuren, N. Kopidakis, P. L. Burn, P. Meredith, *Nat. Commun.* **2015**, *6*, 6343.
[143] Y. Zhong, T. J. Sisto, B. Zhang, K. Miyata, X. Y. Zhu, M. L. Steigerwald, F. Ng, C. Nuckolls, *J. Am. Chem. Soc.* **2017**, *139*, 5644.

[144] B. Siegmund, A. Mischok, J. Benduhn, O. Zeika, S. Ullbrich, F. Nehm, M. Böhm, D. Spoltore, H. Fröb, C. Körner, K. Leo, K. Vandewal, *Nat. Commun.* **2017**, *8*, 15421.
[145] Y. Yao, Y. Chen, H. Wang, P. Samorì, *SmartMat* **2020**, *1*, e1009.
[146] P.-A. Bouit, C. Aronica, L. Toupet, B. Le Guennic, C. Andraud, O. Maury, *J. Am. Chem. Soc.* **2010**, *132*, 4328.
[147] M. Eskandari, J. C. Roldao, J. Cerezo, B. Milián-Medina, J. Gierschner, *J. Am. Chem. Soc.* **2020**, *142*, 2835.
[148] D. Yang, D. Ma, *Adv. Opt. Mater.* **2019**, *7*, 1800522.
[149] Y. Fang, A. Armin, P. Meredith, J. Huang, *Nat. Photonics* **2019**, *13*, 1.
[150] S. Dähne, *Chimia* **1991**, *45*, 288.
[151] R. C. Nelson, *J. Opt. Soc. Am.* **1956**, *46*, 10.
[152] H. Zhang, S. Jenatsch, J. De Jonghe, F. Nüesch, R. Steim, A. C. Véron, R. Hany, *Sci. Rep.* **2015**, *5*, 9439.
[153] A. C. Véron, H. Zhang, A. Linden, F. Nüesch, J. Heier, R. Hany, T. Geiger, *Org. Lett.* **2014**, *16*, 1044.
[154] J. Suddard-Bangsund, C. J. Traverse, M. Young, T. J. Patrick, Y. Zhao, R. R. Lunt, *Adv. Energy Mater.* **2016**, *6*, 1501659.
[155] M. Young, J. Suddard-Bangsund, T. J. Patrick, N. Pajares, C. J. Traverse, M. C. Barr, S. Y. Lunt, R. R. Lunt, *Adv. Opt. Mater.* **2016**, *4*, 1028.
[156] R. D. Jansen-van Vuuren, A. Pivrikas, A. K. Pandey, P. L. Burn, *J. Mater. Chem. C* **2013**, *1*, 3532.
[157] D. M. Lyons, A. Armin, M. Stolterfoht, R. C. R. Nagiri, R. D. Jansen-van Vuuren, B. N. Pal, P. L. Burn, S.-C. Lo, P. Meredith, *Org. Electron.* **2014**, *15*, 2903.
[158] S. Namba, Y. Hishiki, *J. Phys. Chem.* **1965**, *69*, 774.
[159] H. Gerischer, *Faraday Discuss. Chem. Soc.* **1974**, *58*, 219.
[160] B. J. Walker, A. Dorn, V. Bulović, M. G. Bawendi, *Nano Lett.* **2011**, *11*, 2655.
[161] Y. Yang, T. Nakamichi, H. Yoshioka, M. Yahiro, M. Era, H. Watanabe, Y. Cui, Y. Oki, G. Qian, *J. Mater. Chem. C* **2013**, *1*, 1739.
[162] T. P. Osedach, A. Iacchetti, R. R. Lunt, T. L. Andrew, P. R. Brown, G. M. Akselrod, V. Bulović, *Appl. Phys. Lett.* **2012**, *101*, 113303.
[163] S. B. Anantharaman, K. Strassel, M. Diethelm, A. Gubicza, E. Hack, R. Hany, F. A. Nüesch, J. Heier, *J. Mater. Chem. C* **2019**, *7*, 14639.
[164] F. A. Castro, A. Faes, T. Geiger, C. F. O. Graeff, M. Nagel, F. Nüesch, R. Hany, *Synth. Met.* **2006**, *156*, 973.
[165] R. Hany, B. Fan, F. A. de Castro, J. Heier, W. Kylberg, F. Nüesch, *Prog. Photovoltaics* **2011**, *19*, 851.
[166] M. Lenes, H. J. Bolink, *ACS Appl. Mater. Interfaces* **2010**, *2*, 3664.
[167] H. Mustroph, *Phys. Sci. Rev.* **2021**. https://doi.org/10.1515/psr-2020-0145.
[168] S. R. Marder, J. W. Perry, G. Bourhill, C. B. Gorman, B. G. Tiemann, K. Mansour, *Science* **1993**, *261*, 186.
[169] F. Würthner, G. Archetti, R. Schmidt, H.-G. Kuball, *Angew. Chem., Int. Ed.* **2008**, *47*, 4529; *Angew. Chem.* **2008**, *120*, 4605.
[170] F. Würthner, C. Thalacker, R. Matschiner, K. Lukaszuk, R. Wortmann, *Chem. Commun.* **1998**, 1739.
[171] C. Brückner, F. Würthner, K. Meerholz, B. Engels, *J. Phys. Chem. C* **2017**, *121*, 4.
[172] K. Kudo, T. Moriizumi, *Appl. Phys. Lett.* **1981**, *39*, 609.
[173] S. R. Marder, B. Kippelen, A. K. Y. Jen, N. Peyghambarian, *Nature* **1997**, *388*, 845.
[174] F. Würthner, R. Wortmann, R. Matschiner, K. Lukaszuk, K. Meerholz, Y. DeNardin, R. Bittner, C. Bräuchle, R. Sens, *Angew. Chem., Int. Ed.* **1997**, *36*, 2765; *Angew. Chem.* **1997**, *109*, 2933.
[175] F. Würthner, R. Wortmann, K. Meerholz, *ChemPhysChem* **2002**, *3*, 17.
[176] A. Liess, L. Huang, A. Arjona-Esteban, A. Lv, M. Gsänger, V. Stepanenko, M. Stolte, F. Würthner, *Adv. Funct. Mater.* **2015**, *25*, 44.
[177] L.-Y. Lin, Y.-H. Chen, Z.-Y. Huang, H.-W. Lin, S.-H. Chou, F. Lin, C.-W. Chen, Y.-H. Liu, K.-T. Wong, *J. Am. Chem. Soc.* **2011**, *133*, 15822.
[178] Y.-H. Chen, L.-Y. Lin, C.-W. Lu, F. Lin, Z.-Y. Huang, H.-W. Lin, P.-H. Wang, Y.-H. Liu, K.-T. Wong, J. Wen, D. J. Miller, S. B. Darling, *J. Am. Chem. Soc.* **2012**, *134*, 13616.
[179] A. Liess, A. Lv, A. Arjona-Esteban, D. Bialas, A.-M. Krause, V. Stepanenko, M. Stolte, F. Würthner, *Nano Lett.* **2017**, *17*, 1719.
[180] V. Steinmann, N. M. Kronenberg, M. R. Lenze, S. M. Graf, D. Hertel, K. Meerholz, H. Bürckstümmer, E. V. Tulyakova, F. Würthner, *Adv. Energy Mater.* **2011**, *1*, 888.
[181] A. Ojala, A. Petersen, A. Fuchs, R. Lovrincic, C. Pölking, J. Trollmann, J. Hwang, C. Lennartz, H. Reichelt, H. W. Höffken, A. Pucci, P. Erk, T. Kirchartz, F. Würthner, *Adv. Funct. Mater.* **2012**, *22*, 86.
[182] M. G. Han, K.-B. Park, X. Bulliard, G. H. Lee, S. Yun, D.-S. Leem, C.-J. Heo, T. Yagi, R. Sakurai, T. Ro, S.-J. Lim, S. Sul, K. Na, J. Ahn, Y. W. Jin, S. Lee, *ACS Appl. Mater. Interfaces* **2016**, *8*, 26143.
[183] X. Bulliard, Y. W. Jin, G. H. Lee, S. Yun, D.-S. Leem, T. Ro, K.-B. Park, C.-J. Heo, R.-I. Satoh, T. Yagi, Y. S. Choi, S.-J. Lim, S. Lee, *J. Mater. Chem. C* **2016**, *4*, 1117.
[184] G. H. Lee, X. Bulliard, S. Yun, D.-S. Leem, K.-B. Park, K.-H. Lee, C.-J. Heo, I.-S. Jung, J.-H. Kim, Y. S. Choi, S.-J. Lim, Y. W. Jin, *Opt. Express* **2019**, *27*, 25410.
[185] Y. Lim, S. Yun, D. Minami, T. Choi, H. Choi, J. Shin, C.-J. Heo, D.-S. Leem, T. Yagi, K.-B. Park, S. Kim, *ACS Appl. Mater. Interfaces* **2020**, *12*, 51688.
[186] A. Lv, M. Stolte, F. Würthner, *Angew. Chem., Int. Ed.* **2015**, *54*, 10512; *Angew. Chem.* **2015**, *127*, 10658.
[187] A. Liess, A. Arjona-Esteban, A. Kudzus, J. Albert, A. M. Krause, A. Lv, M. Stolte, K. Meerholz, F. Würthner, *Adv. Funct. Mater.* **2019**, *29*, 1805058.
[188] T. Schembri, J. H. Kim, A. Liess, V. Stepanenko, M. Stolte, F. Würthner, *Adv. Opt. Mater.* **2021**, *9*, 2100213.
[189] U. Mayerhöffer, M. Gsänger, M. Stolte, B. Fimmel, F. Würthner, *Chem. - Eur. J.* **2013**, *19*, 218.
[190] U. Mayerhöffer, F. Würthner, *Angew. Chem., Int. Ed.* **2012**, *51*, 5615; *Angew. Chem.* **2012**, *124*, 5713.
[191] S. Spencer, J. Cody, S. Misture, B. Cona, P. Heaphy, G. Rumbles, J. Andersen, C. Collison, *J. Phys. Chem. C* **2014**, *118*, 14840.
[192] F. Balzer, H. Kollmann, M. Schulz, G. Schnakenburg, A. Lützen, M. Schmidtmann, C. Lienau, M. Silies, M. Schiek, *Cryst. Growth Des.* **2017**, *17*, 6455.
[193] M. Schulz, M. Mack, O. Kolloge, A. Lützen, M. Schiek, *Phys. Chem. Chem. Phys.* **2017**, *19*, 6996.
[194] M. Schulz, F. Balzer, D. Scheunemann, O. Arteaga, A. Lützen, S. C. J. Meskers, M. Schiek, *Adv. Funct. Mater.* **2019**, *29*, 1900684.
[195] J. Zablocki, M. Schulz, G. Schnakenburg, L. Beverina, P. Warzanowski, A. Revelli, M. Grüninger, F. Balzer, K. Meerholz, A. Lützen, M. Schiek, *J. Phys. Chem. C* **2020**, *124*, 22721.
[196] M. Binda, T. Agostinelli, M. Caironi, D. Natali, M. Sampietro, L. Beverina, R. Ruffo, F. Silvestri, *Org. Electron.* **2009**, *10*, 1314.
[197] M. Binda, A. Iacchetti, D. Natali, L. Beverina, M. Sassi, M. Sampietro, *Appl. Phys. Lett.* **2011**, *98*, 073303.
[198] G. M. Somashekharappa, C. Govind, V. Pulikodan, M. Paul, M. A. G. Namboothiry, S. Das, V. Karunakaran, *J. Phys. Chem. C* **2020**, *124*, 21730.
[199] K. Strassel, A. Kaiser, S. Jenatsch, A. C. Véron, S. B. Anantharaman, E. Hack, M. Diethelm, F. Nüesch, R. Aderne, C. Legnani, S. Yakunin, M. Cremona, R. Hany, *ACS Appl. Mater. Interfaces* **2018**, *10*, 11063.
[200] K. Strassel, W.-H. Hu, S. Osbild, D. Padula, D. Rentsch, S. Yakunin, Y. Shynkarenko, M. Kovalenko, F. Nüesch, R. Hany, M. Bauer, *Sci. Technol. Adv. Mater.* **2021**, *22*, 194.

[201] W. Li, D. Li, G. Dong, L. Duan, J. Sun, D. Zhang, L. Wang, *Laser Photonics Rev.* **2016**, *10*, 473.
[202] W. Li, H. Guo, Z. Wang, G. Dong, *J. Phys. Chem. C* **2017**, *121*, 15333.
[203] H. Guo, L. Jiang, K. Huang, R. Wang, S. Liu, Z. Li, X. Rong, G. Dong, *Org. Electron.* **2021**, *92*, 106122.
[204] W. Ziegenbein, H.-E. Sprenger, *Angew. Chem., Int. Ed.* **1966**, *5*, 893; *Angew. Chem.* **1966**, *78*, 937.
[205] P. H. Wöbkenberg, J. G. Labram, J.-M. Swiecicki, K. Parkhomenko, D. Sredojevic, J.-P. Gisselbrecht, D. M. de Leeuw, D. D. C. Bradley, J.-P. Djukic, T. D. Anthopoulos, *J. Mater. Chem.* **2010**, *20*, 3673.
[206] F. Arca, M. Sramek, S. F. Tedde, P. Lugli, O. Hayden, *IEEE J. Quantum Electron.* **2013**, *49*, 1016.
[207] L. Beverina, M. Crippa, P. Salice, R. Ruffo, C. Ferrante, I. Fortunati, R. Signorini, C. M. Mari, R. Bozio, A. Facchetti, G. A. Pagani, *Chem. Mater.* **2008**, *20*, 3242.
[208] S. Bellani, A. Iacchetti, M. Porro, L. Beverina, M. R. Antognazza, D. Natali, *Org. Electron.* **2015**, *22*, 56.
[209] Z. Chen, A. Lohr, C. R. Saha-Möller, F. Würthner, *Chem. Soc. Rev.* **2009**, *38*, 564.
[210] H. Wang, Y. Zhang, Y. Chen, H. Pan, X. Ren, Z. Chen, *Angew. Chem., Int. Ed.* **2020**, *59*, 5185; *Angew. Chem.* **2020**, *132*, 5223.
[211] Y. Zhang, P. Liu, H. Pan, H. Dai, X.-K. Ren, Z. Chen, *Chem. Commun.* **2020**, *56*, 12069.
[212] W. Zhao, Z. He, B. Z. Tang, *Nat. Rev. Mater.* **2020**, *5*, 869.
[213] L. Zhang, H.-X. Wang, S. Li, M. Liu, *Chem. Soc. Rev.* **2020**, *49*, 9095.
[214] R. Naaman, D. H. Waldeck, *Ann. Rev. Phys. Chem.* **2015**, *66*, 263.
[215] J. R. Brandt, F. Salerno, M. J. Fuchter, *Nat. Rev. Chem.* **2017**, *1*, 0045.
[216] L. Zhang, I. Song, J. Ahn, M. Han, M. Linares, M. Surin, H.-J. Zhang, J. H. Oh, J. Lin, *Nat. Commun.* **2021**, *12*, 142.
[217] J. Gierschner, S. Varghese, S. Y. Park, *Adv. Opt. Mater.* **2016**, *4*, 348.
[218] Y. Jiang, Y.-Y. Liu, X. Liu, H. Lin, K. Gao, W.-Y. Lai, W. Huang, *Chem. Soc. Rev.* **2020**, *49*, 5885.
[219] T. Byrnes, N. Y. Kim, Y. Yamamoto, *Nat. Phys.* **2014**, *10*, 803.
[220] M. Y. Lee, H. R. Lee, C. H. Park, S. G. Han, J. H. Oh, *Acc. Chem. Res.* **2018**, *51*, 2829.
[221] M. R. Wasielewski, M. D. E. Forbes, N. L. Frank, K. Kowalski, G. D. Scholes, J. Yuen-Zhou, M. A. Baldo, D. E. Freedman, R. H. Goldsmith, T. Goodson, M. L. Kirk, J. K. McCusker, J. P. Ogilvie, D. A. Shultz, S. Stoll, K. B. Whaley, *Nat. Rev. Chem.* **2020**, *4*, 490.

Jin Hong Kim studied at the Department of Material Science and Engineering of Seoul National University where he received the Ph.D. degree in 2019 for his research with Prof. Soo Young Park on field-effect transistors and phototransistors based on 2D organic semiconductors. After a post-doctoral stay at Seoul National University (2019–2020), he joined Prof. Frank Würthner's group at the Center of Nanosystems Chemistry (CNC) in Würzburg as a postdoctoral researcher in 2020. Here his research focus is on organic photodetectors based on dye aggregates.

Tim Schembri received his M.Sc. in functional materials at the University of Würzburg (Germany) in 2020 and is currently a Ph.D. candidate at the Center for Nanosystems Chemistry (CNC) in Würzburg under supervision of Prof. Frank Würthner. His main research interest lies in the field of organic electronics with research experience in organic solar cells, photodiodes, electrochromics, and solid-state emitters.

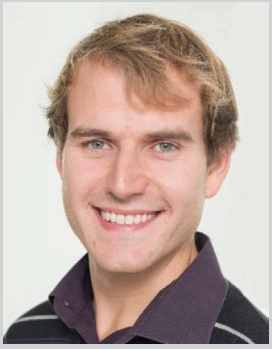

David Bialas studied chemistry at the University of Würzburg (Germany) and received his Ph.D. under the supervision of Prof. Frank Würthner in 2017. After a postdoctoral stay at Temple University in Philadelphia (USA) in the group of Prof. Frank Spano (2018–2019), he continued as a research associate in the group of Prof. Frank Würthner. His main research interest is to theoretically investigate the optical properties of dye aggregates.

Matthias Stolte studied chemistry at the University of Kaiserslautern, Germany and finished his Ph.D. thesis in 2008 under the guidance of Prof. Hans-Georg Kuball. Afterward he joined the group of Prof. Frank Würthner at the University of Würzburg as postdoctoral fellow and focused his research on organic colorants and their application in organic electronic devices. As senior research associate since 2010 his investigations at the Center for Nanosystems Chemistry focus on the optical and electrical characterization of organic solid-state materials and their application in organic thin-film and single-crystal transistors as well as organic solar cells and photodiodes.

Frank Würthner studied chemistry at the University of Stuttgart (doctoral degree 1994) and continued his career at MIT (postdoc), the University of Ulm (Habilitation 2001) and the University of Würzburg (since 2002). His research interests include the synthesis of functional dyes, the construction of supramolecular photosystems for artificial photosynthesis, and the application of functional π-systems in organic electronics, photonics, and photovoltaics. He is an elected member of the German National Academy of Science Leopoldina and the Bavarian Academy of Sciences. His awards include the Arnold-Sommerfeld-Prize (2002), an ERC Advanced Grant (2017), and the Adolf-von-Baeyer Medal (2019).